Biomedicine & Pharmacotherapy 167 (2023) 115600

Contents lists available at ScienceDirect

Biomedicine & Pharmacotherapy

journal homepage: www.elsevier.com/locate/biopha

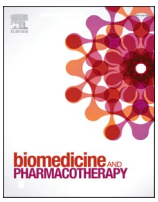

Frentizole derivatives with mTOR inhibiting and senomorphic properties

Zofia Chrienova [a,1], David Rysanek [b,1], Josef Novak [b], Pavla Vasicova [b], Patrik Oleksak [a], Rudolf Andrys [a], Adam Skarka [a], Jelena Dumanovic [c], Zoran Milovanovic [d], Vesna Jacevic [e], Marketa Chvojkova [a,f], Kristina Holubova [a,f], Karel Vales [a,f,g], Veronika Skoupilova [a], Marian Valko [h], Klaudia Jomova [i], Suliman Y. Alomar [j], Fernanda D. Botelho [k], Tanos C.C. Franca [a,k], Kamil Kuca [a], Zdenek Hodny [b,*], Eugenie Nepovimova [a,*]

[a] Department of Chemistry, Faculty of Science, University of Hradec Kralove, Rokitanskeho 62, 500 03 Hradec Kralove, Czech Republic
[b] Department of Genome Integrity, Institute of Molecular Genetics of the Czech Academy of Sciences, Videnska 1083, 142 20 Prague, Czech Republic
[c] Faculty of Chemistry, University of Belgrade, Studenski trg 16, 11000 Belgrade, Serbia
[d] Special Police Unit, Ministry of Interior, Trebevićka 12/A, 11030 Belgrade, Serbia
[e] Department of Experimental Toxicology and Pharmacology, National Poison Control Centre, Military Medical Academy & Medical Faculty of the Military Medical Academy, University of Defence, 11 Crnotravska, 11000 Belgrade, Serbia
[f] National Institute of Mental Health, Topolova 748, 250 67 Klecany, Czech Republic
[g] Third Faculty of Medicine, Charles University, Ruska 87, 100 00 Prague 10, Czech Republic
[h] Faculty of Chemical and Food Technology, Slovak University of Technology in Bratislava, 812 37 Bratislava, Slovakia
[i] Department of Chemistry, Faculty of Natural Sciences and Informatics, Constantine the Philosopher University in Nitra, 949 01 Nitra, Slovakia
[j] Zoology Department, College of Science, King Saud University, Riyadh 11451, Saudi Arabia
[k] Laboratory of Molecular Modeling Applied to Chemical and Biological Defense (LMCBD), Military Institute of Engineering, 22290–270 Rio de Janeiro, RJ, Brazil

ARTICLE INFO

Keywords:
Frentizole
ABAD
MTOR
Cellular senescence
Aging

ABSTRACT

Frentizole is immunosuppressive drug with low acute toxicity and lifespan-prolonging effect. Recently, frentizole's potential to disrupt toxic amyloid β (Aβ) - Aβ-binding alcohol dehydrogenase (ABAD) interaction in mitochondria in Alzheimer's brains has been revealed. Another broadly studied drug with anti-aging and immunosuppressive properties is an mTOR inhibitor – rapamycin. Since we do not yet precisely know what is behind the lifespan-prolonging effect of rapamycin and frentizole, whether it is the ability to inhibit the mTOR signaling pathway, reduction in mitochondrial toxicity, immunosuppressive effect, or a combination of all of them, we have decided within our previous work to dock the entire in-house library of almost 240 Aβ-ABAD modulators into the FKBP-rapamycin-binding (FRB) domain of mTOR in order to interlink mTOR-centric and mitochondrial free radical-centric theories of aging and thus to increase the chances of success. Based on the results of the docking study, molecular dynamic simulation and MM-PBSA calculations, we have selected nine frentizole-like compounds (**1** – **9**). Subsequently, we have determined their real physical-chemical properties (logP, logD, pKa and solubility in water and buffer), cytotoxic/cytostatic, mTOR inhibitory, and *in vitro* anti-senescence (senolytic and senomorphic) effects. Finally, the three best candidates (**4**, **8**, and **9**) have been forwarded for *in vivo* safety studies to assess their acute toxicity and pharmacokinetic properties. Based on obtained results, only compound **4** demonstrated the best results within *in vitro* testing, the ability to cross the blood-brain barrier and the lowest acute toxicity (LD_{50} in male mice 559 mg/kg; LD_{50} in female mice 575 mg/kg).

Abbreviations: ABAD, Aβ-binding alcohol dehydrogenase; AD, Alzheimer's disease; Aβ, amyloid β; BBB, blood-brain barrier; BJ, normal human skin fibroblasts; CVA, crystal violet assay; DIS, drug-induced senescence; DMEM, Dulbecco's modified Eagle's medium; FACS, fluorescence-activated cell sorting; FBS, fetal bovine serum; FRB, FKBP-rapamycin-binding; GFP, green fluorescent protein; HBA, hydrogen-bond acceptor; HBD, hydrogen-bond donor; i.m., intramuscular; i.p, intraperitoneal; IR, ionizing radiation; LD_{50}, median lethal dose; logD, distribution coefficient at pH 7.4; mTOR, mechanistic target of rapamycin; NEAA, NEAA non-essential amino acids; OIS, oncogene-induced senescence; PBS, phosphate buffer solution; pKa, acid-base dissociation constant; polyHEMA, poly(2-hydroxyethyl) methacrylate; RA, resazurin assay; Ro5, Lipinski's "rule of five"; ROS, reactive oxygen species; RPE-1, human non-transformed telomerase-immortalized retinal pigment epithelial cells; RtB, rotatable bonds; S6K, p70 S6 kinase; SASP, senescence-associated secretory phenotype; TMZ, temozolomide; tPSA, polar surface area.

* Corresponding authors.
E-mail addresses: zdenek.hodny@img.cas.cz (Z. Hodny), eugenie.nepovimova@uhk.cz (E. Nepovimova).

[1] Zofia Chrienova and David Rysanek contributed equally.

https://doi.org/10.1016/j.biopha.2023.115600
Received 4 July 2023; Received in revised form 9 September 2023; Accepted 25 September 2023
Available online 30 September 2023

1. Introduction

Cellular senescence is a state of permanent cell cycle arrest that plays an important role in embryogenesis, wound healing, and protection against cancer. [1] It can be triggered by multiple mechanisms, including DNA damage, changes in the epigenetic landscape and gene expression, persistent macromolecular damage and aberrant metabolism, and activation of a hypersecretory phenotype. [2] Together, all these mechanisms limit excessive or aberrant cellular proliferation, so the state of senescence protects against the development of cancer. However, recent data suggest that cellular senescence may also be involved in aging and contribute to the development of chronic, frequently age-related disorders, such as atherosclerosis, type 2 diabetes mellitus, neurodegenerative diseases, or, controversially, cancer. [3] The emerging evidence suggests that the drawbacks of senescence are twofold. First, senescence causes a loss of tissue-repair capacity because of cell cycle arrest in progenitor cells. Second, senescent cells produce several factors, including proinflammatory and matrix-degrading molecules known as the senescence-associated secretory phenotype (SASP). [4] The SASP includes activated interleukins, chemokines, extracellular matrix components, metalloproteinases, growth factors, and other signaling molecules. The SASP proinflammatory signal activates an innate immune response that aims to clear senescent cells. However, a sustained induction of senescence can lead to a large accumulation of senescent cells that triggers a chronic inflammatory state with detrimental effects on neighboring cells in a paracrine manner through a mechanism that generates reactive oxygen species (ROS) and DNA damage. [5,6].

For decades, one of the most debated questions in gerontology has been whether aging is a disease or not. The current agreement is that aging has both programmed (i.e., aging is a continuation of ontogenetic development) and stochastic (i.e., aging is a random accumulation of errors) causal components. [7,8] Since aging could be understood as a disease, thus, it should be potentially treatable. Treatments are generally more effective in the pre-disease phase, associated with hyperfunction, than at disease stages, associated with functional decline. Such preventative anti-aging drugs include statins, aspirin, angiotensin-converting enzyme inhibitors, and metformin. [9] However, the universal cornerstone in anti-aging preventative as well as causal medicine should be highlighted rapamycin, since it shows the ability to reduce late-life pathology. [10] Rapamycin exhibits multiple properties, including antibacterial, antifungal, anticancer, and immunosuppressive effects. All these exceptional properties have been linked to rapamycin's capacity to inhibit large multiprotein complexes with serine/threonine kinase activity, called the mechanistic (earlier mammalian) target of rapamycin (mTOR). [11,12] In 2003, Vellai et al. revealed the role of a mTOR signaling pathway in aging. Indeed, the downregulation of mTOR signaling extends the lifespan of various animal species. [13] In 2009, another study pointed out that treatment of genetically heterogeneous male and female mice with rapamycin may extend the mean and maximal lifespan, despite the initiation of treatment at an advanced age (corresponding to a human age of 60 years). [14].

There are two functionally distinct mTOR complexes, termed mTORC1 and mTORC2. mTORC1 mediates nutrient signals to control diverse cellular processes related to growth and proliferation, while mTORC2 is required for normal actin cytoskeleton organization. [15] Under nutrient-rich conditions, mTORC1 kinase promotes growth, protein translation, and tRNA synthesis. Under starvation conditions, however, mTORC1 inhibition slows down cell proliferation and favors cell maintenance via controlling critical regulators involved in autophagy. [16] All these breakthrough findings led to the formulation of the so-called "mTOR-centric theory of aging". [17] Among the other pillars supporting this hypothesis can be involved the fact that the role of mTOR in lifespan regulation is highly conserved in all eukaryotes, suggesting a universal aging mechanism or the findings that an extremely high proportion of mTOR regulators and effectors also regulate lifespan. [18,19].

Cell growth, regulated partly by mTOR, and cellular senescence, one of the hallmarks of aging, are seemingly two antagonistic biological processes because cell growth is a process of mass accumulation while senescence is the state of arrest. However, emerging data show that these two cellular processes are linked together. Some facts indicate the authenticity of this claim, e.g., 1) the mTOR signaling pathway is hyperactivated in senescent cells; 2) many morphological hallmarks of senescent cells, such as enlarged size, accumulation of mitochondrial and lysosomal mass, etc. are regulated by mTORC1; 3) pharmacological inhibition of mTOR by rapamycin decreases the cellular markers of senescence. [20] Broadly speaking, cellular senescence reflects some, if not all, aspects of organismal aging and age-related diseases and can be modulated by mTOR activity. Therefore, pharmacological targeting of the mentioned kinase by small-molecule inhibitors may represent a unique universal preventative tool to not only slow down aging, but also to prevent/treat neurodegenerative diseases, type 2 diabetes mellitus, or even cancer.

Another hypothesis explaining the etiology of aging is the "mitochondrial free radical theory of aging". [21] A simplified version of this theory is that free radicals such as ROS or hydrogen peroxide produced during mitochondrial respiration cause cumulative damage to DNA, proteins, and lipids in the cell, eventually leading to tissue loss of functionality and, ultimately, organismal death. [18] ROS burden can also be observed in various age-related diseases, e.g., Alzheimer's disease (AD), cardiovascular disorders, etc. [22,23] In the case of AD, the question is whether AD biology mechanistically diverges from aging biology at all or represents exaggerated aging. Particularly in AD, it has been revealed that the interaction of soluble forms of amyloid β (Aβ) peptide with mitochondrial enzyme termed Aβ-binding alcohol dehydrogenase (ABAD) may distort the enzyme's structure, rendering it inactive concerning its cytoprotective properties, and promotes thus mitochondrial generation of free radicals. [24] Probably, the overriding question is not the exact mechanism of ROS contribution to aging and AD but whether free radicals are the major contributors to aging and AD. Unfortunately, the recent findings suggest otherwise. It is worth mentioning, for example, the failure of antioxidant monotherapy in humans to achieve significant health benefits. [25].

2. Design

An interesting study on a murine model of lupus erythematosus treated with frentizole was published in 1982. Apart from drug efficiency, such experiment revealed a prolonged lifespan in studied animals. [26] Frentizole (Fig. 1) is benzimidazoleurea with good immunosuppressive activity and low acute toxicity. [27] One of the most common shortcomings associated with immunosuppressive therapy is a predisposition of ill individuals/persons to various types of infection. However, Scheetz et al. reported that frentizole-treated mice were not predisposed to infections by various agents and, in fact, host resistance was even augmented by frentizole. [28].

The renaissance of frentizole occurred in 2006 when Xie et al. employing a high-throughput screening assay identified frentizole's potential to inhibit Aβ-ABAD interaction. [29] Disruption of such interaction may at least decrease mitochondrial toxicity within aging or even serve as a novel potential therapeutic approach against AD. For a long time, a part of our scientific group has focused on the latter application

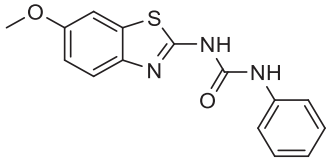

Fig. 1. Chemical structure of frentizole.

of Aβ-ABAD interaction modulators derived from frentizole. Its more than ten-year scientific efforts resulted in the synthesis and biological evaluation of several hundreds of new compounds. [30–35].

Since we do not yet precisely know what causes the lifespan-prolonging effect of rapamycin and frentizole, whether it is the ability to inhibit the mTOR signaling pathway, reduction in mitochondrial toxicity, immunosuppressive effect, or a combination of all of them, we have decided to dock the entire in-house library of almost 240 Aβ-ABAD modulators into the FKBP-rapamycin-binding (FRB) domain of mTOR in order to interlink mTOR-centric and mitochondrial free radical-centric theories of aging and thus to increase the chances of success (Chart 1). [36] Based on the results of this docking study, molecular dynamic simulation and MM-PBSA calculations, we have managed to select nine frentizole-like compounds (**1** – **9**, Fig. 2) with the lowest binding energy to the FRB domain of mTOR. Subsequently, we have determined their real physical-chemical properties, cytotoxic/cytostatic, mTOR inhibitory, and *in vitro* anti-senescence (senolytic and senomorphic) effects. The inhibitory effect of **1** – **9** and frentizole towards ABAD has been published earlier. [31–33] Finally, the three best candidates (**4**, **8**, and **9**) have been forwarded for *in vivo* safety studies to assess their acute toxicity and pharmacokinetic properties. Additionally, since mTOR inhibitors have been evaluated in many preclinical and clinical trials against cancer, [37–39] we have decided to test the target compounds also for their anti-cancer potential.

3. Results and discussion

3.1. Synthesis

Synthetic procedures describing the preparation of selected compounds (**1** – **9**) have been already published. [30,32,33].

3.2. Physicochemical properties determination

Pharmacologically active lead compounds should maintain their drug-like physicochemical properties during the process of selectivity and activity optimization. All molecules in this study (**1** – **9**) were assessed by generally used Lipinskiś "rule of five" (Ro5), the rule of thumb that estimates drug-likeness and ascertains whether the chemical and physical properties of a particular compound would provide an orally effective drug or not. The Ro5 as a computational and experimental technique predicts that poor absorption or permeation of a drug is more probable when the molecule fulfills two or more of the criteria: (a) the molecular weight is greater than 500; (b) calculated or experimental logP is greater than 5; (c) there are more than 5 hydrogen-bond donors (HBD); (d) there are more than 10 hydrogen-bond acceptors (HBA). [40].

Considering our compounds, molecular weight, HBD, and HBA were computed by ACDLAbs PhysChemSuite software. The calculated results are listed in Table 1. In our set of studied molecules, molecular weight ranged from 360.82 (**2**) to 438.21 (**4**), indicating that none of our molecules exceeded the 500 Da criterion. Moreover, none of the molecules exerted HBD or HBA values greater than the estimated limit; the values ranged from 2 to 4 and 4 – 8, respectively. The logP values were determined by the shake-flask method, and obtained data ranged from 2.58 (**7**) to 6.25 (**1**) (Table 1). Three of nine molecules (**1**, **2**, **3**) showed experimentally measured logP values greater than five.

Additional descriptors of drug-like properties that link the permeability of the compound with the molecular flexibility were proposed by Veber et al. [41] He concluded that the number of rotatable bonds (RtB) exceeding 10 generally correlates with poor permeability. He also indicated that permeability is affected by high polar surface area (tPSA), and this descriptor must exert values smaller than 140 Å^2. All of the

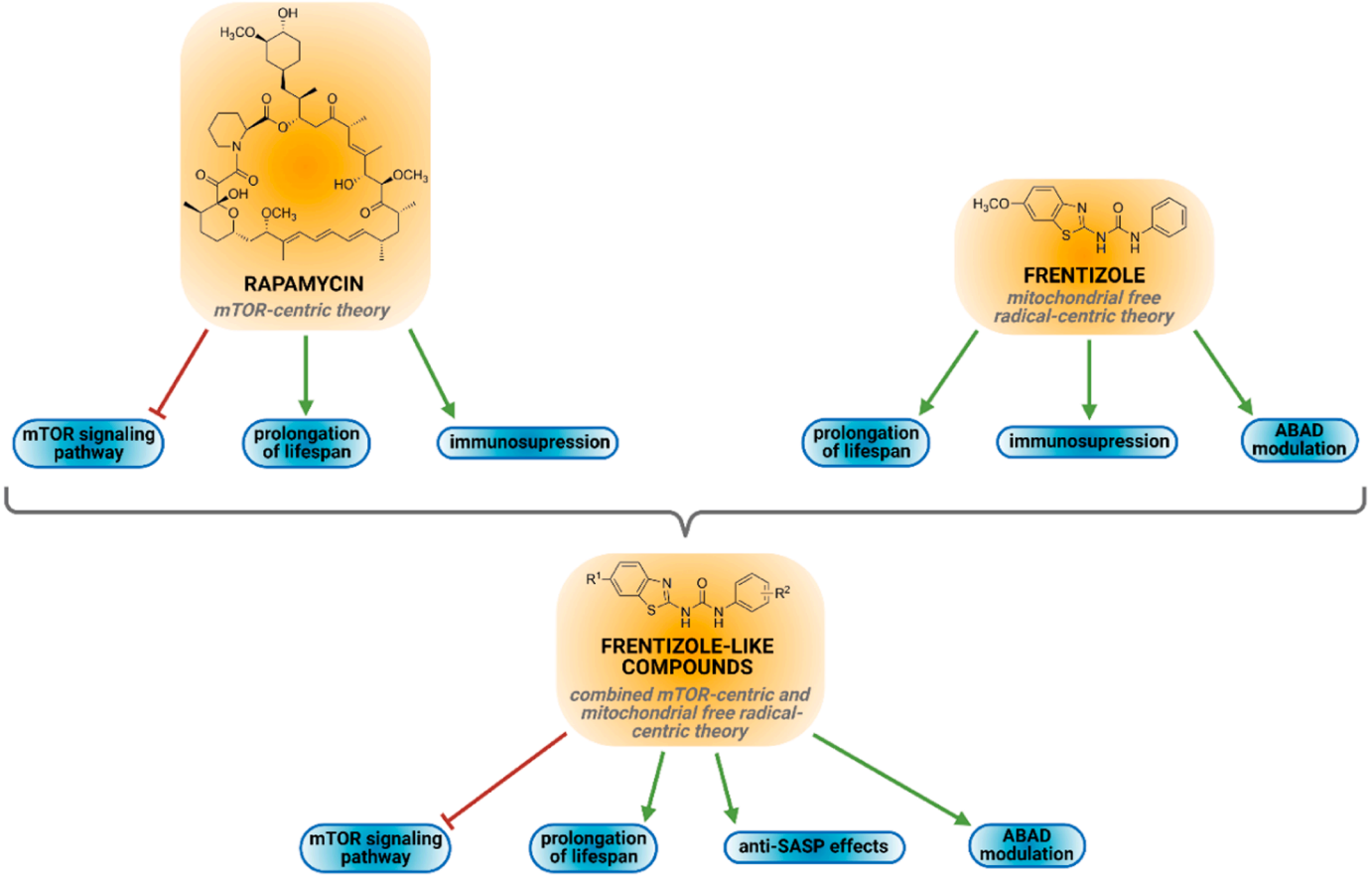

Chart 1. The design strategy of the novel anti-aging approach.

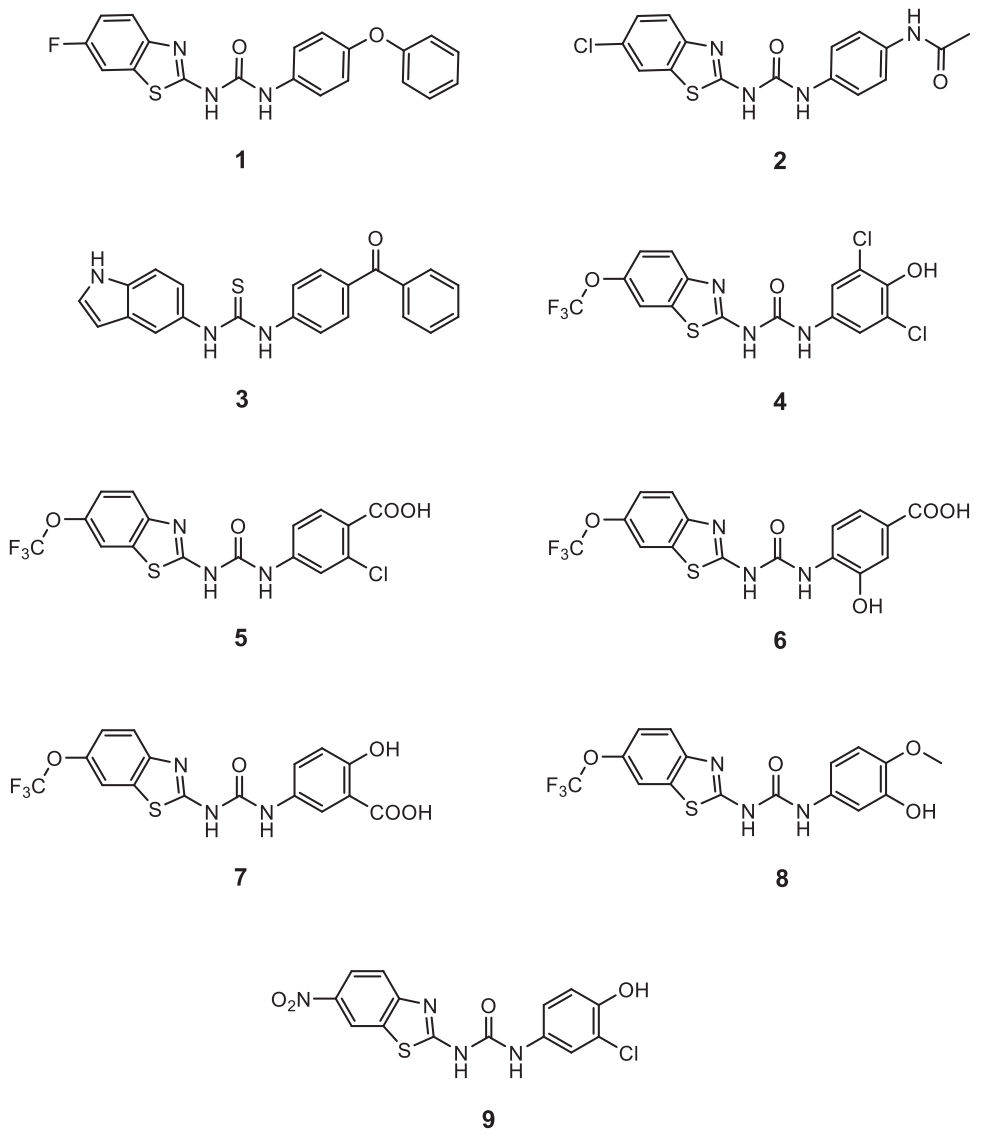

Fig. 2. Chemical structure of frentizole-like compounds selected by the foregoing computational study.

Table 1
Drug-like physicochemical properties of studied molecules.

Name	Mw	logP	HBD	HBA	RtB	tPSA (Å^2)
1	379.41	6.25 ± 0.01	2	5	4	91.49
2	360.82	5.85 ± 0.03	3	6	3	111.36
3	371.46	5.82 ± 0.01	3	4	6	89.01
4	438.21	4.04 ± 0.17	3	6	4	111.72
5	431.77	3.29 ± 0.06	3	7	5	128.79
6	413.33	2.72 ± 0.18	4	8	5	149.02
7	413.33	2.58 ± 0.04	4	8	5	149.02
8	399.35	4.59 ± 0.25	3	7	5	120.95
9	364.76	4.78 ± 0.10	3	8	3	151.32

studied compounds had 10 or fewer rotatable bonds; the number ranged from 3 (**2** and **9**) to 6 (**3**) (Table 1). Except for **6**, **7**, and **9**, all of the molecules demonstrated a polar surface area of less than 140 Å^2; tPSA values ranged from 89.01 (**3**) to 151.32 (**9**) (Table 1).

Since the acid-base dissociation constant (pKa) of a drug influences lipophilicity, permeability, solubility, and protein binding and is considered an important factor affecting pharmacokinetic characteristics, this parameter was determined as well. A spectrophotometric titration was used to obtain experimental pKa values of all nine molecules with the distribution of the required values from 4.31 (**5**) to 10.27 (**8**) (Table 2). However, due to poor solubility in water, the titration was performed in 50% methanol to maintain homogeneous solutions. Under given conditions, **3** was not dissolved sufficiently; thus, the pKa value of this compound was not determined.

For the complex characterization of given molecules, the distribution coefficient at pH 7.4 (logD) and solubility in water and buffer with pH 7.4 were assessed (Table 2). Obtained experimental logD values ranged from 1.71 (**7**) to 6.27 (**1**). Since moderate logD (0−3) is optimal for oral absorption and membrane permeation, compounds **5**, **6**, and **7** fulfilled the criterion and fell into the group of appropriate candidates. The high logD value (>3) of the remaining seven compounds is also associated with their low solubility, erratic absorption, and potential high plasma binding. [41] Performed nephelometry assay reported very poor solubility of all nine compounds in both water and buffer with pH 7.4. In particular, all compounds demonstrated solubility in water lower than 6 μg/mL and an average $\log S_{H2O}$ value lower than (−4.82). In addition, solubility in buffer solution with pH 7.4 was lower than 6 μg/mL, and an average $\log S_{pH7.4}$ was lower than (−4.81) for six molecules (**1**, **2**, **3**, **4**, **8**, **9**). Remaining three compounds (**5**, **6**, **7**) exerted solubility in buffer 104.7 μg/mL, 12.8 μg/mL, and 349.3 μg/mL and $\log S_{pH7.4}$ values (−3.62), (−4.51), and (−3.07), respectively.

Table 2
Dissociation constants, distribution coefficients and solubility values of studied compounds.

Name	pKa1	pKa2	logD	Sol. $_{(H2O)}$ (μg/mL)	$logS_{H2O}$	Sol. $_{(pH\ 7.4)}$ (μg/mL)	$logS_{pH7.4}$
1	7.39 ± 0.24	10.26 ± 0.02	6.27 ± 0.01	< 6	< −4.80	< 6	< −4.80
2	7.23 ± 0.19	9.82 ± 0.03	5.85 ± 0.06	< 6	< −4.78	< 6	< −4.78
3	n/a	n/a	5.82 ± 0.01	< 6	< −4.79	< 6	< −4.79
4	6.64 ± 0.25	10.24 ± 0.20	4.18 ± 0.14	< 6	< −4.86	< 6	< −4.86
5	4.31 ± 0.07	8.22 ± 0.12	1.86 ± 0.01	< 6	< −4.86	104.7	-3.62
6	5.16 ± 0.16	8.52 ± 0.27	2.33 ± 0.09	< 6	< −4.84	12.8	-4.51
7	7.09 ± 0.26	10.17 ± 0.13	1.71 ± 0.06	< 6	< −4.84	349.3	-3.07
8	7.14 ± 0.21	10.27 ± 0.10	4.48 ± 0.25	< 6	< −4.82	< 6	< −4.82
9	6.69 ± 0.32	10.15 ± 0.17	4.82 ± 0.04	< 6	< −4.78	< 6	< −4.78

n/a value not obtained due to poor solubility

In conclusion, all compounds showed very favorable absorption and permeation properties when assessed by Ro5, except for **1**, **2**, and **3,** which failed to conform to one out of four rules. When additional characteristics proposed by Veber et al. (RtB and tPSA) are added to the assessment, compounds **4**, **5**, and **8** met all specified conditions. However, only compound **5** showed optimal logD values in addition to the

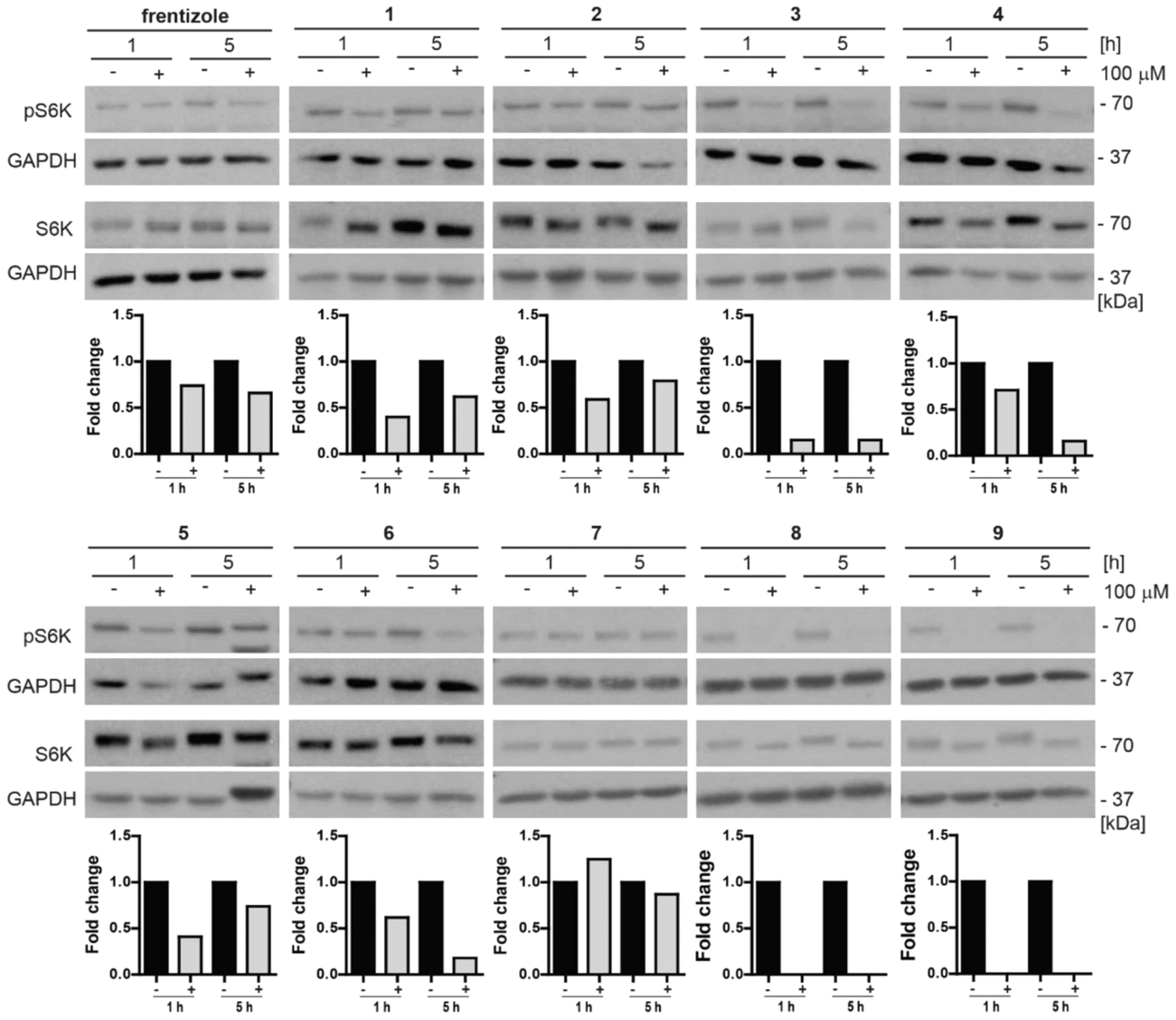

Fig. 3. Inhibition of mTORC1 kinase by frentizole and its derivatives. BJ cells were exposed to 100 μM concentration of compounds **1** – **9** for 1 and 5 h and the level of p70 S6 kinase (S6K) threonine 389 (Thr389) phosphorylation mediated by mTORC1 and S6K total level were detected by immunoblotting with specific antibodies. GAPDH was used as a loading control. Quantitative analysis of immunoblots was done by ImageJ 1.48 v program with GAPDH as the internal control. The experiment was done in duplicate.

previously mentioned descriptors. Since none of the tested molecules showed a fitting solubility profile, there is no "perfect candidate" emerging from obtained data. Nevertheless, Ro5 and other descriptors serve merely as helping tools in the decision-making process. Even rapamycin, one of the most used mTOR inhibitors, does not meet the given conditions, and the final decision about candidates for *in vivo* experiments should consider *in vitro* activity, as well as physicochemical properties.

3.3. Biological properties

3.3.1. Inhibition of mTORC1 kinase activity in proliferating and senescent cells

To investigate the mTORC1 kinase inhibitory activity of frentizole and its derivatives, normal human skin fibroblasts (BJ) cells were selected as the most sensitive to mTORC1 inhibition compared to other cell types used in this study (see below). The level of mTORC1-mediated phosphorylation of its substrate p70 S6 kinase (S6K) was assayed in BJ cells exposed to 100 μM of the tested compound for one and five hours by immunoblotting. Unlike frentizole exhibiting a relatively mild inhibition of threonine 389 (Thr389) S6K phosphorylation, frentizole derivatives, except compound **7**, showed an apparent inhibitory effect on S6K phosphorylation (Fig. 3). Compounds **3**, **4**, and **6**, and, namely, compounds **8** and **9**, were the most potent inhibitors of S6K phosphorylation. Note that the effect on S6K phosphorylation was associated with faster electrophoretic mobility of S6K caused by the absence of S6K phosphorylation.

This data confirms/supports in conditions *in vitro* the results of *in silico* study [36] that frentizole and its selected derivatives could bind to the FRB domain of mTOR kinase and inhibit its enzymatic activity in an allosteric rapamycin-like manner. Thus, besides ABAD inhibitory activity, we identified mTOR as their novel molecular target that could be pharmacologically utilizable.

To obtain the 'minimal' inhibitory concentration of the most potent compounds **4**, **8**, and **9**, BJ cells were exposed to the concentration range of 0 – 100 μM for 1 and 5 h. The level of S6K phosphorylation was determined by immunoblotting as above (Fig. 4). The observable S6K phosphorylation was detected at 6.25 μM for compound **4** (1 and 5 h), 12.5 μM for compound **8** (5 h), and 25 μM for compound **9** (1 and 5 h).

Senescent cells are thought to contribute to aging and age-associated diseases, including AD (see, e.g., [42,43]). Therefore, eliminating senescent cells or modulating their adverse effects is an emerging target of anti-aging strategies (reviewed in [44]). To compare the inhibition of mTORC1 kinase in proliferating and senescent cells, we exposed both proliferating and senescent cells to compounds **4**, **8**, and **9** and determined the level of p70 S6K phosphorylation by immunoblotting (Fig. 5). Compared to non-transformed telomerase-immortalized retinal pigment epithelial (RPE-1) cells, BJ cells were overall more sensitive to the inhibitory effect of all three compounds irrespective of the cell state (i.e., proliferation or senescence). No significant differences in p70 S6K phosphorylation among the three compounds were observed, though compounds **8** and **9** appeared slightly more effective in inhibiting p70 S6K phosphorylation than compound **4**. No substantial differences between oncogene- and drug-induced senescence in BJ cells were revealed. For ionizing radiation (IR)-senescent RPE-1 cells, the lowest inhibitory effect on p70 S6K phosphorylation was found for compound **9**.

Together, our findings indicate that compounds **4**, **8**, and **9** can inhibit mTORC1-mediated phosphorylation of its substrate p70 S6K both in proliferating and senescent cells. However, cell type-dependent differences in sensitivity to mTORC1 inhibition can be observed.

3.4. Effects of novel frentizole derivatives on inflammatory cytokines production

Senescent cells produce a specific secretome termed senescence-associated secretory phenotype, comprising several groups of proteins, including pro-inflammatory cytokines. [45] The SASP is being intensively studied as a factor contributing to the pathogenesis of age-associated diseases, including cancer. [46] As several components of SASP are under mTOR control, [47] next we determined the effect of frentizole and its derivatives on expression of selected components of SASP. Culture media conditioned by IR-induced RPE-1 senescent cells were analyzed for the level of 11 pro-inflammatory cytokines IL-1α, IL-1β, IL-6, IL-8, IL-10, IL-12p70, IL-27, MCP-1, IFNγ, TNFα, and IP-10 by fluorescence-activated cell sorting (FACS) analysis after 24 h-long incubation of senescent cells with frentizole and its derivatives (Fig. 6). The concentration of individual substances was adjusted to avoid a cytotoxic effect (see the legend in Fig. 8 for the compound concentration used). Overall, the frentizole and its derivatives showed variable effects on individual cytokine levels compared to untreated senescent cells (Table 3). To summarize, the levels of IL-1α/β remained nearly unaffected by compounds **1** – **6**. There was a tendency for upregulation of IL-8 (two-fold on average, except compound **6**), IL-10 (three-fold on average, except compounds **1** and **7**), IL-27 (two-fold on average, except compounds **1** – **6** and frentizole), TNFα (three-fold on average, except compound **6**), and IP-10 (two-fold on average, for compounds **2**, **9**, and frentizole).

Importantly, IL-6, a cytokine with complex immunomodulatory and malignant feature-promoting functions (reviewed in [48]), tends to be downregulated by most of the tested substances, with the exception of compound **2**. In addition, most compounds revealed the robust downregulation of MCP-1, a key chemokine regulating migration and infiltration of monocytes and macrophages and emerging as an anticancer target, [49] though the effect was less pronounced for compounds **6** and **7** compared to the rest of the derivatives. Marked downregulation was also observed in the case of IL-12p70, a key immunomodulatory cytokine in innate and adaptive immune response (for a review, see [50]), in cells exposed to compounds **7** – **9**.

The general conclusion, which can be drawn from these observations, is that several frentizole derivatives can affect the secretome of senescent cells. The most promising observed effect was on the downregulation of IL-6, MCP-1, and IL-12p70 produced by radiation-induced senescent cells, where the compounds **4**, **8**, and **9** scored effectively in suppression of all these three proinflammatory cytokines. Given that the composition of SASP depends on several conditions, including complex cell-to-cell interactions in tissues, it is difficult to interpret the physiological role of frentizole derivatives on SASP suppression without further detailed explorations in *in vivo*.

The red arrow indicates the decrease, the empty field shows no change, and the green arrow the increase of cytokine level in all three replicates.

3.5. Determination of antiproliferative effects of frentizole and its derivatives in vitro

The effect on cell proliferation of all nine compounds, including frentizole as a reference compound, was examined *in vitro* on human proliferating cells using normal BJ fibroblasts, RPE-1, and cancerous glioblastoma U373 cells. The cells were exposed to the compounds at concentrations of 0, 10, 50, 80, and 100 μM for 24 h. First, crystal violet (CVA) and resazurin assays (RA) were used as indirect indicators of cell viability (Fig. 7). Contrary to the absence of antiproliferative effects of frentizole assayed by CVA, most frentizole derivatives, except compound **2**, affected cell growth in a cell type-dependent manner. Compounds **1**, **3**, **4**, **8**, and **9** scored as the most potent antiproliferative frentizole derivative, even on cancerous glioblastoma cell line U373 (Fig. 7A-C). Similar results for compounds **1**, **3**, **4**, **8**, and **9** were obtained by RA. However, all other compounds showed at least a mild effect on metabolic activity, including frentizole (Fig. 7D-F). We found a statistically significant correlation between inhibition of p70 S6K phosphorylation and cytotoxic effect (Pearson correlation coefficient 0.6494, p-value 0.04214; determined for BJ cells).

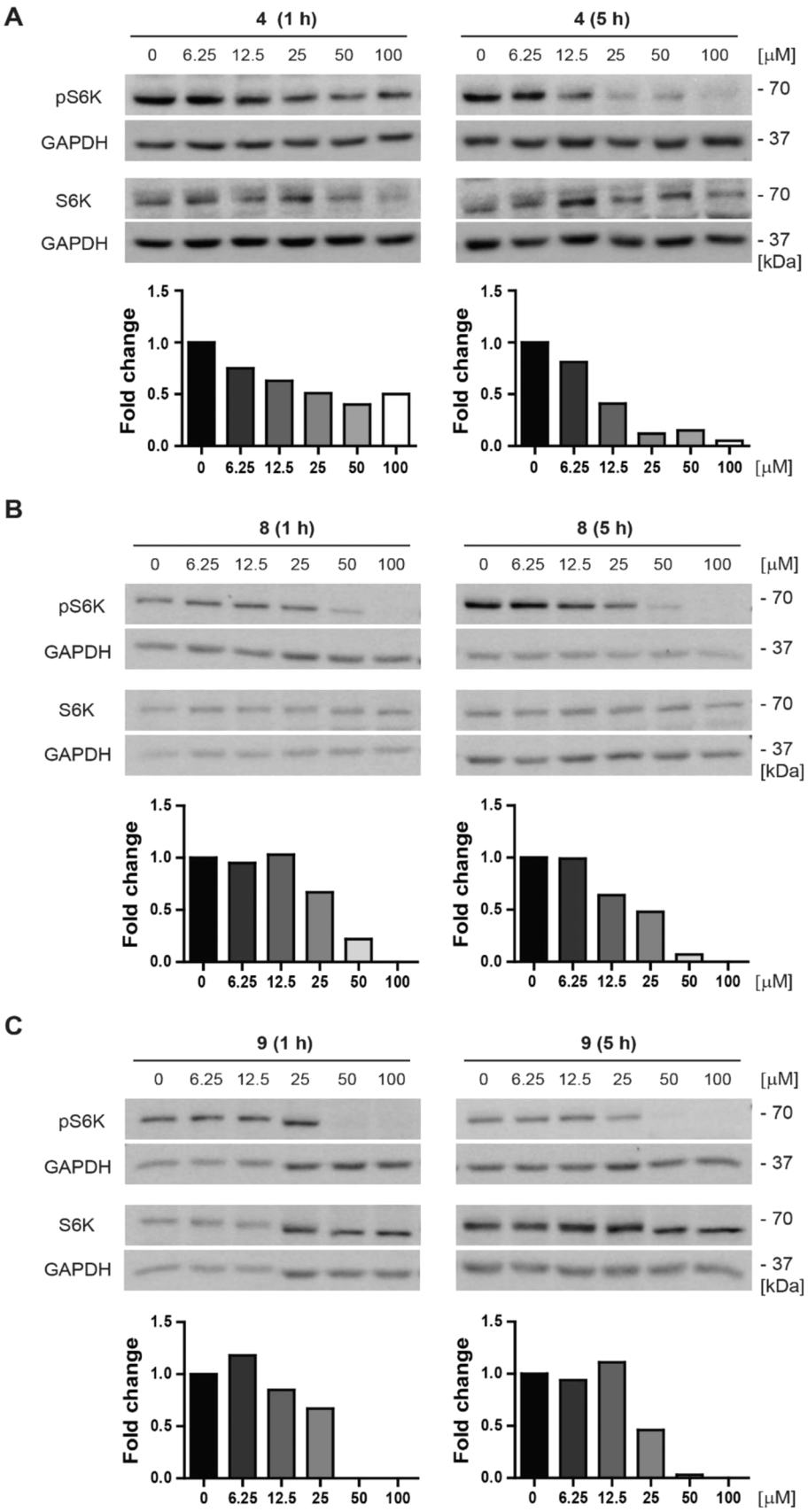

Fig. 4. Determination of minimal mTORC1 kinase inhibitory concentration of selected compounds 4, 8, and 9. BJ cells were exposed to compounds **4**, **8**, and **9** in the concentration range of 0 – 100 μM for 1 and 5 h. The levels of phospho-p70 S6K (Thr389) and total p70 S6K were determined by immunoblotting. GAPDH was used as a loading control. Quantitative analysis of immunoblots was done by ImageJ 1.48 v program with GAPDH as the internal control.

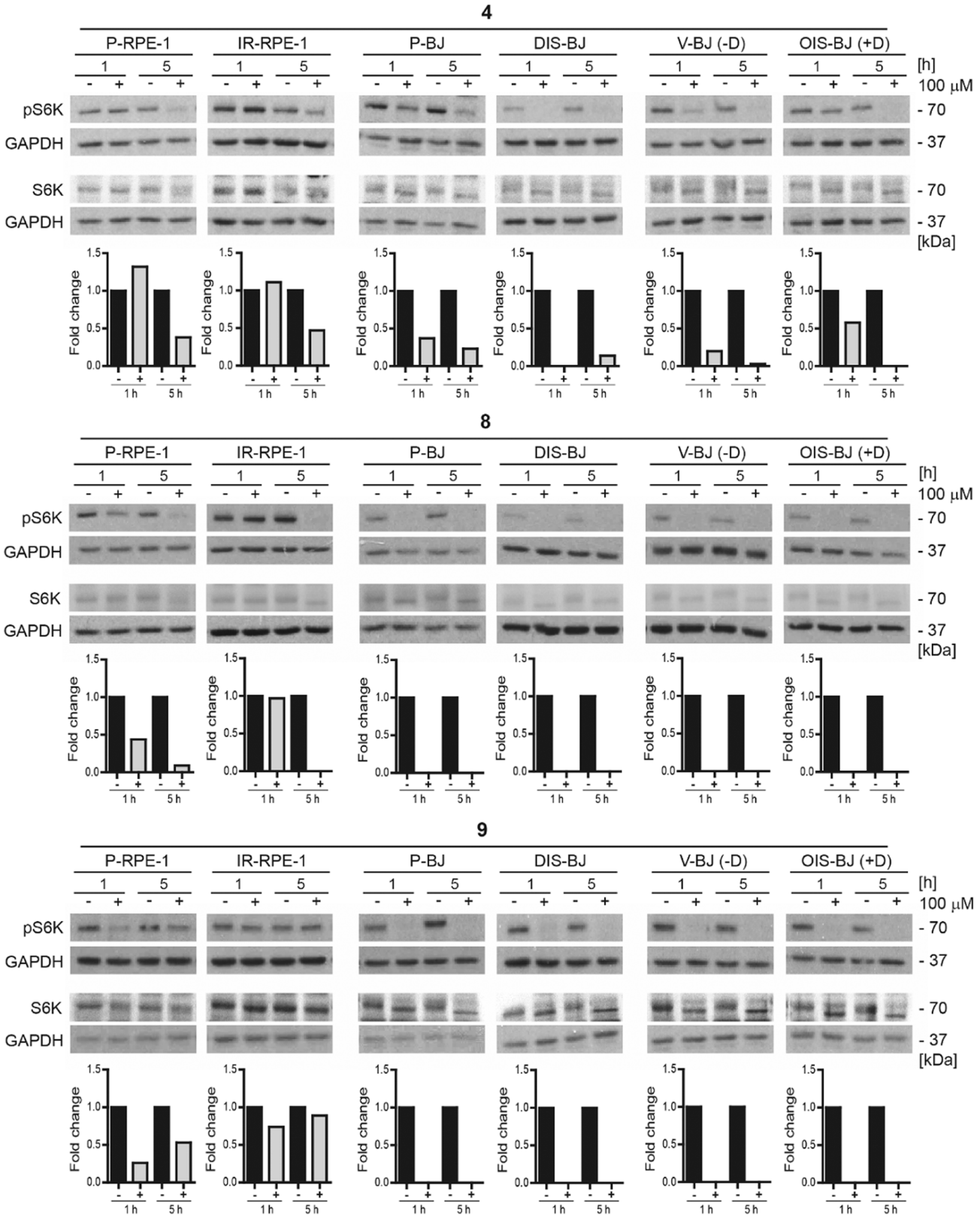

Fig. 5. Comparison of mTORC1 kinase inhibitory effect of selected compounds 4, 8, and 9 in proliferating and senescent cells. Proliferating RPE-1 (P-RPE-1), BJ (P-BJ) and BJ cells transduced with oncogenic Ras vector (V-BJ(-D)) prior to induction of Ras oncogene with doxycycline were compared to senescent cells: IR-induced RPE-1(IR-RPE-1), docetaxel-induced (DIS-BJ), and Ras-induced (OIS-BJ (+D)) BJ. Cells were exposed to compounds **4**, **8**, and **9** (100 μM) for 1 and 5 h. The level of phospho-p70 S6K (Thr389) and total p70 S6K were determined by immunoblotting. GAPDH was used as a loading control. Quantitative analysis of immunoblots was done by ImageJ 1.48 v program with GAPDH as the internal control.

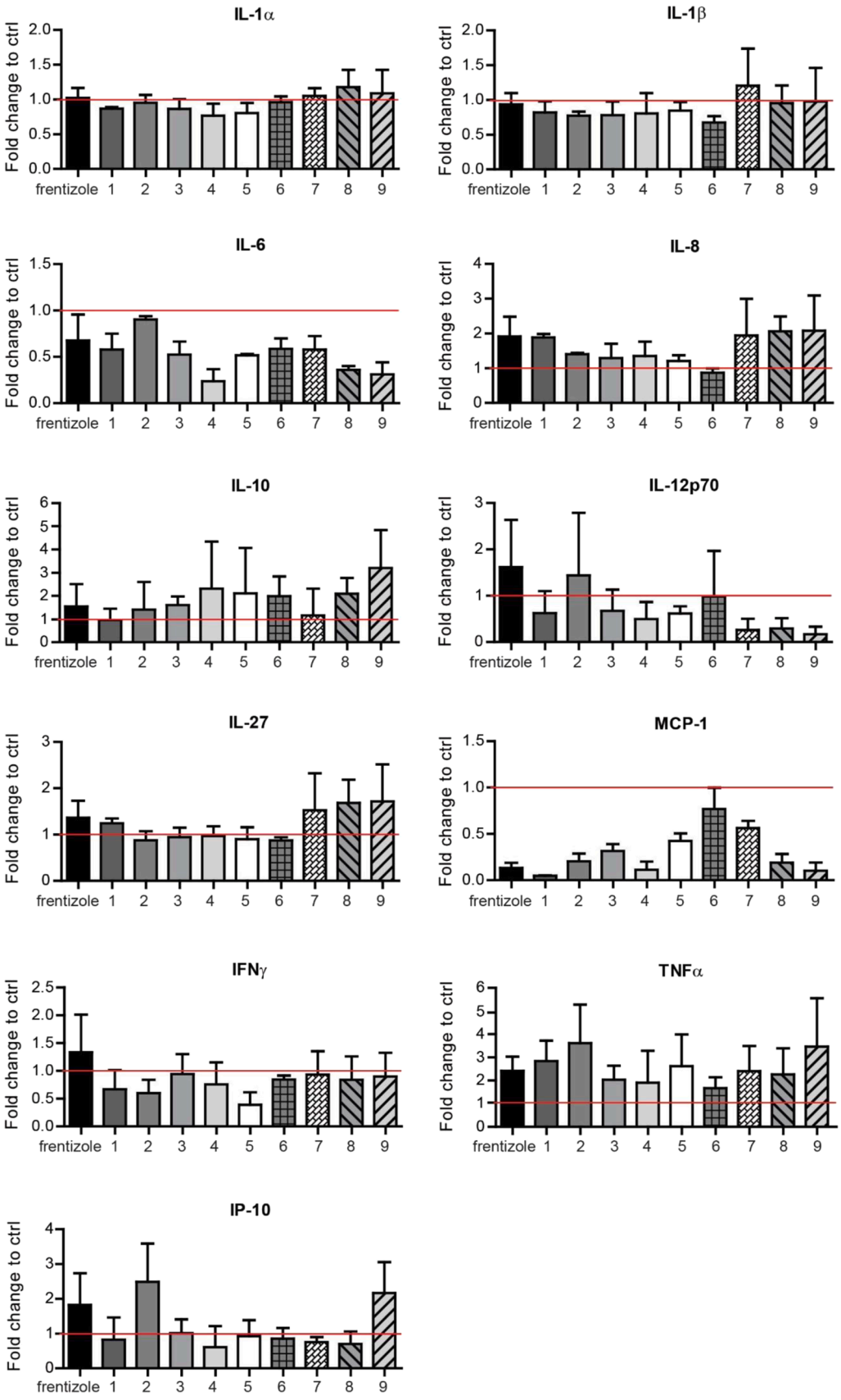

(caption on next page)

Fig. 6. Effect of frentizole and its derivatives on the secretion of pro-inflammatory cytokines in the ionizing radiation-induced senescent cells. IR-induced senescent RPE-1 cells (20 Gy, 7 days) were exposed to compounds **1** – **9** for 24 h. Frentizole was used as a reference compound. Conditioned media were collected 24 h after cell treatment and analyzed for the level of pro-inflammatory cytokines IL-1α, IL-1β, IL-6, IL-8, IL-10, IL-12p70, IL-27, MCP-1, IFNγ, TNFα, and IP-10 by FACS analysis. The concentration of compound used: 100 μM for **1**, **2**, **3**, **4**, **5**, **6**, and **7**, 80 μM for **9**, and 50 μM for **8**. The experiment was done in triplicate. Data were normalized to untreated cells as fold induction to control (set as 1 – red line) and plotted as mean ± SEM.

Table 3
Effect of frentizole and its derivatives on the secretion of pro-inflammatory cytokines in the ionizing radiation-induced senescent cells.

	IL-1α	IL-1β	IL-6	IL-8	IL-10	IL-12p70	IL-27	MCP-1	IFNγ	TNFα	IP-10
frentizole			▼					▼		▲	▼
1	▼	▼	▼	▲			▲	▼		▲	
2		▼	▼	▲				▼	▼	▲	▲
3	▼	▼	▼		▲			▼		▲	
4	▼		▼					▼			
5	▼	▼	▼			▼		▼	▼		
6		▼	▼				▼		▼	▲	
7			▼			▼		▼			▼
8			▼	▲		▼		▼			
9			▼			▼		▼			▲

These findings indicate that the mTOR inhibitory activity of frentizole derivatives is associated with growth suppressive properties, as expected for mTOR inhibition (reviewed, e.g., in [51]).

3.6. Senolytic activity of novel frentizole derivatives

Compared to their proliferating predecessors, senescent cells are more resistant to apoptosis. [52] To investigate the senolytic effect of frentizole derivatives, we employed three models of premature cellular senescence, i.e., drug-(docetaxel, DIS), oncogene-(H-Ras, OIS), and IR-induced senescence triggered in normal (BJ) and non-transformed immortalized (RPE-1) cells *in vitro* (see Experimental section). Frentizole did not exert any cytotoxic effect on senescent cells as evaluated by the CVA (Fig. 8A–C), whereas a mild but significant effect detected by RA was observed only for OIS in BJ cells. However, for its derivatives (**1** – **9**), the cytotoxicity of most compounds against senescent cells was similar to the effect on proliferating cells. Compound **8** harbored the most consistent cytotoxic effect for all types of senescent cells in both assays. The selective senolytic effect (i.e., higher toxicity against senescent than proliferating cells) was observed in cell type- and senescence inductor-specific manner for compounds **1** and **9** (i.e., specifically for docetaxel-induced senescent BJ fibroblasts, SI, Fig. S1A-D). Discrepancies in the results obtained with CVA and RA for senescent cells are due to the latter being rather metabolic than a viability test. Besides the impact on cell viability, the results of RA can be influenced by essential changes in energetic metabolism during senescence development. [53].

In conclusion, frentizole derivatives generally did not exhibit the selective senolytic effect. However, the absence of selectivity is not incapacitating them as potential senolytics.

3.7. Selected frentizole derivatives induce apoptosis in proliferating non-transformed and cancerous cells

We selected compounds **4**, **8**, and **9** for further testing based on their optimal physical-chemical properties and scoring in the above assays. To discriminate between the cytostatic and cytotoxic effects of compounds **4**, **8**, and **9** (used in the concentration range 10 – 100 μM), first, we followed how they affect proliferation of RPE-1 cells by time-lapse microscopy using the Incucyte SX1 platform. The proliferation curves shown in Fig. 9A-C showed an apparent concentration-dependent antiproliferative effect of all three compounds during 72-hour exposure. The positive staining for annexin V was indicative of cell death. As the time-lapse microscopy does not allow proper quantification of the apoptotic cells due to their release from a focal plane, the FACS analysis for apoptosis with annexin V/Hoechst 33258 staining confirmed the presence of apoptosis in a concentration-dependent manner in all three RPE-1 cell cultures exposed to compounds **4**, **8**, and **9** for 24 h (see scatter plot on the right side of Fig. 9). Compound **8** was the most pro-apoptotic, as the findings of CVA and RA indicated. Frentizole showed negligible effect on apoptosis induction (data not shown). A similar cytotoxic effect was confirmed for the glioblastoma U373 cell line (SI, Fig. S2A-D). These results showed that selected frentizole derivatives **4**, **8**, and **9** affected cell growth at lower concentrations with the induction of regulated cell death at higher concentrations, which agrees with rapamycin's reported effects *in vitro*. [54].

3.8. Selected frentizole derivatives induce senolytic effect in senescent cells

As viability tests (RA and CVA, see Fig. 8) indicated a potential senolytic effect of frentizole derivatives, therefore we again employed time-lapse microscopy combined with apoptosis fluorescence markers to prove cytotoxic activity of compounds **4**, **8**, and **9** against normal senescent cells. As shown in Fig. 10, all three compounds used in the concentration range 10 – 100 μM showed an apparent dose-dependent effect on the survival of IR-induced senescent RPE-1 cells after 72-hour exposure, confirmed by FACS analysis of annexin V/Hoechst 33258 staining (24 h). A similar response was found for docetaxel-induced senescent BJ cells (SI, Fig. S3). This data unequivocally showed the presence of regulated cell death in senescent cells triggered by compounds **4**, **8**, and **9**. Thus, in concert with the effect of rapamycin, which is reported to show predominantly the senomorphic effect modulating the SASP without triggering cell death at low concentration and cell death at higher concentration, [55,56] compounds **4**, **8**, and **9** possess both senomorphic and senolytic action.

3.9. Compound 4 exerts cytotoxicity on human glioblastoma proliferating cells

As compound **4** exerted the best physicochemical properties to cross the blood-brain barrier (BBB) combined with good biological properties,

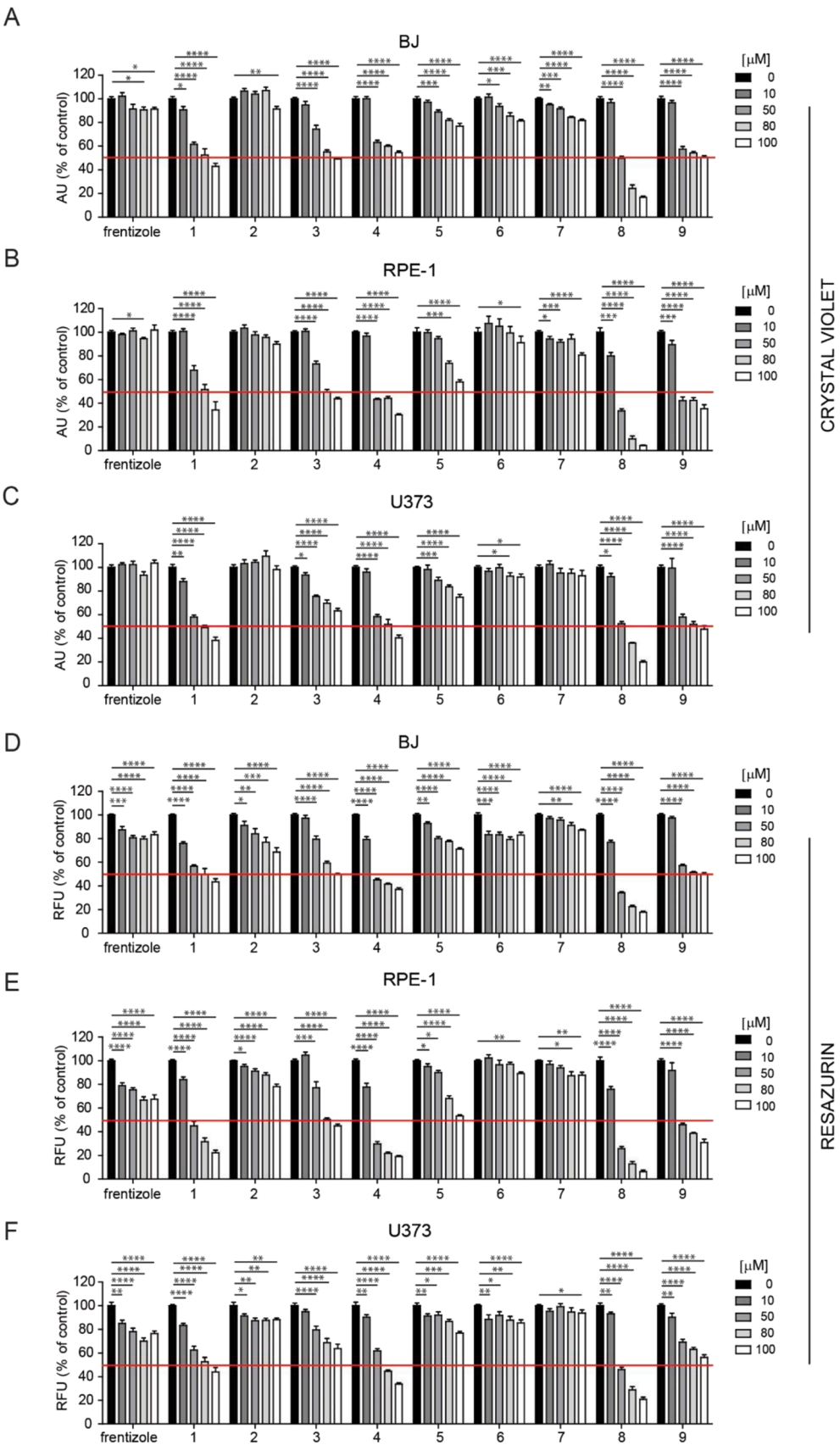

(caption on next page)

Fig. 7. The antiproliferative effect of frentizole-derived compounds. Human BJ fibroblasts (**A**, **D**), immortalized retinal pigment epithelium RPE-1 (**B**, **E**), and glioblastoma U373 (**C**, **F**) cell lines were exposed to compounds **1** – **9** in a concentration range of 0 – 100 μM for 24 h. Frentizole was used as a reference compound. Cell density and metabolic activity were determined by crystal violet (A, B, C) and resazurin (D, E, F) assays, respectively. The experiment was done in triplicate. Data were normalized to untreated cells and plotted as mean ± SEM. Student's t-test, * ** *, $p < 0.0001$; * ** , $p < 0.001$; * *, $p < 0.01$; * , $p < 0.05$. Red lines indicate 50% 'viability' compared to untreated control.

we further examined its effects in the context of human glioblastoma cell lines. Using time-lapse microscopy and FACS analysis to follow cell proliferation and cell death of A172, T98, and U87 glioblastoma cell lines exposed to concentration 10 – 100 μM of compound **4** for 0 – 72 h, there was an evident cytotoxic effect on all three lines, even on T98 considered as particularly resistant (Fig. 11A, B, SI, Fig. S4A-C).

Furthermore, as 2D cell cultures are known to reflect the cytotoxicity in tissues poorly, we employed a 3D spheroid culture of U87 cells expressing green fluorescent protein (U87/GFP) (Fig. 11C, D). The growth suppression of compound **4** followed for 168 h was observable from the concentration of 10 μM above by the decrease of fluorescence intensity of U87/GFP spheroids (see graph in Fig. 11D).

Collectively, these results indicated that compound **4** evinces cytotoxicity against human glioblastoma cells in 2D cultures. This effect was further confirmed using 3D tumor spheroid model of glioblastoma U87/GFP cells.

3.10. Compound 4 harbors a senolytic effect on human glioblastoma senescent-like cells

As the senescent-like phenotype is a common outcome of chemotherapy, including temozolomide (TMZ)-treated glioblastoma, [57] we examined the effect of compound **4** on TMZ-induced senescent-like U87/GFP cells. Time-lapse microscopy and FACS analysis of TMZ-induced senescent-like U87/GFP cells revealed the dose-dependent cytotoxic effect of compound **4** used in the 10 – 100 μM concentration range for 72 and 24 h, respectively (Fig. 12A, B). A noticeable dose- and time-dependent senolytic effect was also observed for 3D spheroids composed of TMZ-induced senescent-like U87/GFP cells exposed to compound **4** in the concentration range of 10 – 100 μM (Fig. 12C).

This data indicates compound **4** to be effective in regulated cell death induction in proliferating and senescent-like glioblastoma cells.

3.11. Compound 4 synergizes the cytotoxic effect of temozolomide on glioblastoma cell lines

Last, to examine whether a combination of compound **4** with TMZ could possess additive/synergic action on the survival of cancer cells, glioblastoma A172, T98, U87, and U373 cells were exposed to a combination matrix of TZM (0 – 200 μM) and compound 4 (0 – 100 μM) concentrations (see SI, Fig. S5) for 72 h. Besides the general additive effect, synergism between both compounds was observed for specific concentrations (i.e., 10 μM compound **4** combined with 100 – 200 μM temozolomide), namely for A172, and U87 (Fig. 13). Only weak synergy between both compounds was found for T98, and U373 cells. Together, these findings indicate that combined treatment of glioblastoma cells with compound **4** and TMZ augmented the TMZ cytotoxicity. This observation is in concert with synergistic effect of rapamycin on cell death of human glioma cell line U251 exposed to TMZ. [58] Whether frentizole derivatives can overcome the resistance of glioma stem cells to TMZ by downregulation of SOX2 and SOX9, as was reported for rapamycin, [59] warrants further investigation.

3.12. Determination of the median lethal dose (LD_{50}) in mice

Determination of acute toxicity of any drug candidate plays an important role in the evaluation of its pharmacological and toxicological profile. The promising approach for acute toxicity evaluation (i.e., LD_{50}) in mice is using a single dose of the compound wherein lethality is determined within 24-hour of studies. [60,61] When compared to mice, some adverse effects and systemic toxicity may occur due to species differences, sex dependence, individual variations, and regulation. The rapid absorption of the drug via the intraperitoneal (i.p.) route enables an easy entry into the circulation, thereby showing the immediate effect. Thus, based on the results obtained within the *in vitro* experiments, frentizole-like compounds **4**, **8**, and **9** have been selected and forwarded for such *in vivo* safety studies.

The noticeable signs of acute toxicity in rodents were not observed when exposed to a low dose of **4**, **8**, and **9**. The first clinical signs of intoxication, such as muscle pain, tenderness, weakness, and tremors, could be seen in all mice up to 2 h after administration of the mild dose of each compound. The severity of these signs was related to the dose concentration. The first side effects without death were also noticed in mice 4 h after each administration at a dose higher than 50% LD_{50}. All mice treated with two of the highest single doses of each compound showed the most intensive muscle pain, convulsions, dyspnea, and tremors during 24 h. Moreover, when exposed to sublethal doses of **4**, **8**, and **9**, all mice showed no signs of toxicity. Accordingly, noticeable signs of toxicity have not been observed in the surviving animals during the 14 days of observation. Survived animals were in good shape. Their hair, skin, visible mucosa, muscle tonicity, movements, and coordination were preserved.

The first lethal effects occurred after administration of a single mid-dose of **4**, **8**, and **9** in mice. Among the treated animals with the highest dose of each compound, it was found that some animals died immediately after a few minutes. However, the rest of the treated mice were drowsy and less responsive, and the death occurred within 2–4 h after administration of each compound. The highest single dose of **4**, **8**, and **9** induced a 100% mortality rate after 24 h.

Overall, the results in Tables 4 – 6 demonstrate that the most favorable toxicity profile was achieved for compound **4** (LD_{50} in male mice 559 mg/kg; LD_{50} in female mice 575 mg/kg). Additionally, the calculated LD_{50} values of **4**, **8**, and **9** clearly show that all the selected compounds exerted lower toxicity in female mice after i.p. administration than in male mice, indicating gender differences.

3.13. Pharmacokinetic study

To investigate the basic pharmacokinetic properties of **4**, **8**, and **9**, the compounds were injected into mice (1 mg/kg i.p.), and their concentrations in the plasma and brain tissue were analyzed at the time points of 15, 30, 60, 180 min and 24 h. The results are depicted in Fig. 14.

The analysis of the drug concentrations in plasma gave the following results. The maximum plasma concentrations of **4** and **9** were reached in the 30th min (c_{max} = 7.223 ± 3.665 ng/mL and 2.520 ± 0.838 ng/mL, respectively), while the maximum plasma concentration of **8** was reached in the 15th minute after administration (c_{max} = 9.222 ± 2.689 ng/mL). Unlike **8** and **9**, whose plasma concentrations dropped to zero 3 h after administration, a detectable plasma level of **4** was present 3 h and, although very low, even 24 h after the administration.

Of the three studied compounds, only **4** was able to reach the brain, being detected there between the 15th and 180th minutes after i.p. administration, while in the case of **8**, only a marginal concentration was present in the brain in the 30th min (0.006 ± 0.010 ng/mL). Finally, regarding **9**, there were no detectable levels in the brain tissue at any time point. The compound **4** rapidly entered the brain and over the time, its concentration in the brain seemed to parallel that in plasma.

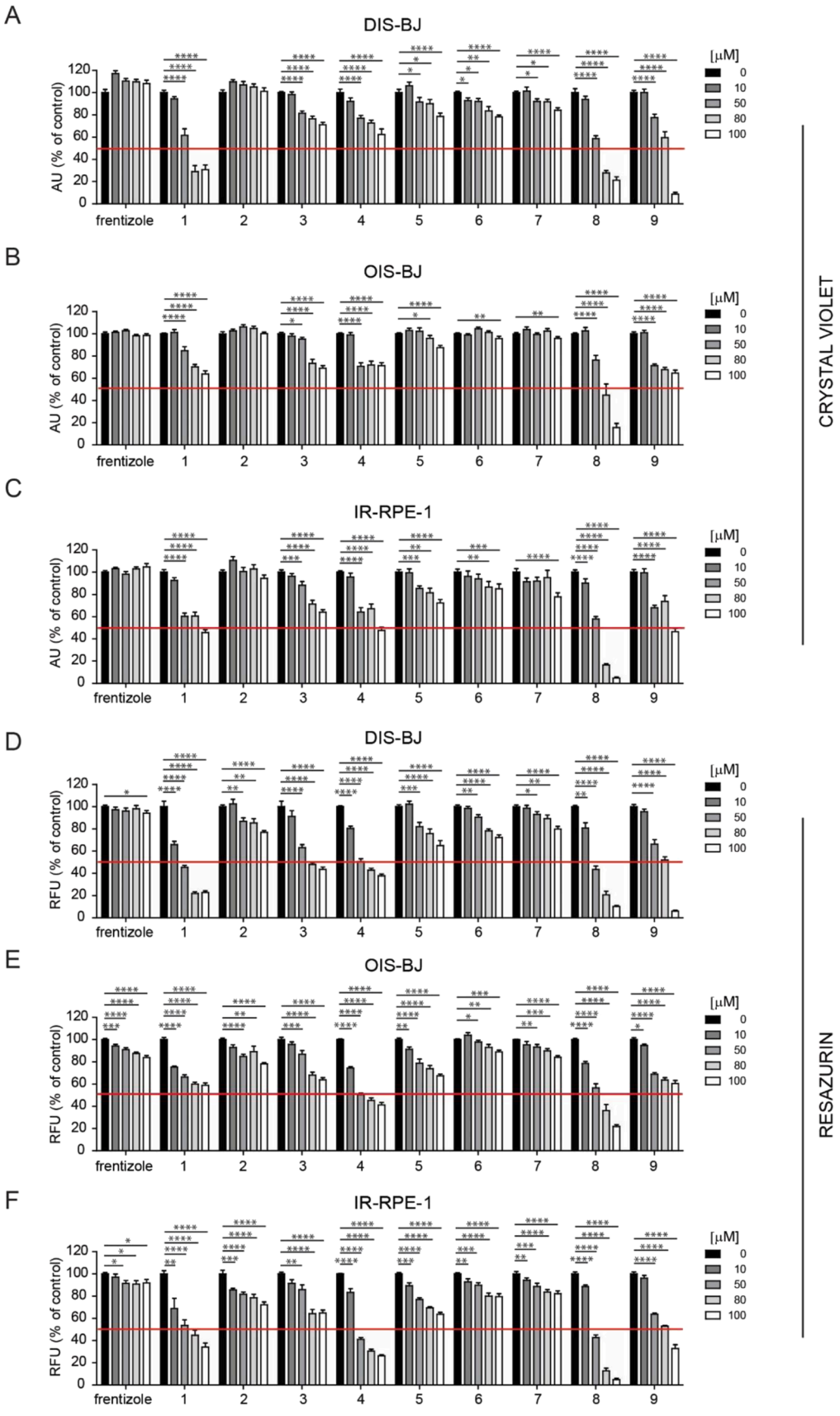

(caption on next page)

Fig. 8. The senolytic effect of frentizole derivatives. Human BJ fibroblasts brought to docetaxel- (DIS; **A**, **D**) and oncogene- (OIS; **B**, **E**) induced senescence, and human immortalized retinal pigment epithelium RPE-1 cells set to ionizing radiation-induced senescence (IR; **C**, **F**) were exposed to compounds **1** – **9** in a concentration range of 0 – 100 μM for 24 h. Frentizole was used as a reference compound. Cell density and metabolic activity were determined by crystal violet (A, B, C) and resazurin (D, E, F) assays, respectively. The experiment was done in triplicate. Data were normalized to untreated cells and plotted as mean ± SEM. Student's t-test, * ** *, $p < 0.0001$; * ** , $p < 0.001$; * *, $p < 0.01$; * , $p < 0.05$. Red lines indicate 50% 'viability' compared to untreated control.

Nevertheless, the blood-brain barrier penetration was limited, as the brain levels were considerably (about 20 times) lower than the plasma levels. The maximum brain concentration of **4** was reached in the 30th min ($c_{max} = 0.261 \pm 0.148$ ng/mL).

In conclusion, analyzing the basic pharmacokinetic properties of **4**, **8**, and **9** revealed that only **4** was centrally available.

4. Conclusion

Aging is the most significant risk factor for most chronic diseases, accounting for most morbidity and healthcare expenditures in developed nations. Therefore, targeting aging itself might be a better strategy than targeting each chronic disease individually to enhance human health. New findings suggest that aging is a modifiable risk factor, and it may be feasible to delay age-related diseases as a group by modulating fundamental aging mechanisms. One such mechanism is cellular senescence, which can cause chronic inflammation via the senescence-associated secretory phenotype.

Within our contribution, we have focused on repurposing experimental modulators of the toxic Aβ-ABAD interaction derived from frentizole for their anti-aging senomorphic effect. Based on the results of molecular docking, molecular dynamic simulation and MM-PBSA calculations, nine lead structures were selected for biological evaluation. All nine compounds and a comparative standard frentizole were forwarded to evaluate the ability to inhibit mTORC1-mediated phosphorylation of its substrate p70 S6K in both proliferating and senescent cells. After that, the effect of **1** – **9** on a specific secretome produced by senescent cells, the so-called SASP, was determined. Both experiments highlighted compounds **4**, **8**, and **9** as the most promising drug candidates for inducing the downregulation of IL-6, MCP-1, and IL-12p70 produced by senescent cells. Subsequently, using time-lapse microscopy combined with apoptosis fluorescence markers, it was found that selected frentizole derivatives **4**, **8**, and **9** induce senolytic effects in senescent cells. Pursuant to the fact that senotherapeutics are studied not only from the perspective of aging, but also of cancer, we have decided to subject compound **4**, exerting the best results in the experiment above, for a more detailed investigation concerning glioblastoma. The results of these assays revealed that substance **4** exerts the cytotoxic effect on human glioblastoma proliferating cells and synergizes the cytotoxic action of temozolomide on glioblastoma cell lines. Last but not least, the three best candidates, i.e., **4**, **8**, and **9**, were forwarded for *in vivo* evaluation. The determination of the acute toxicity and pharmacokinetic study in mice highlighted compound **4** as the only substance able to cross the blood-brain barrier and, at the same time, exerting the lowest toxicity in mice (LD_{50} = 559 mg/kg for males and LD_{50} = 576 mg/kg for female, respectively).

If the premise is correct that targeting senescent cells of the SASP can delay or prevent multiple age-related chronic diseases as a group rather than one at a time, and if the positive preclinical results of **4** can be translated into clinical treatment, we would be optimistic that health care as we know it might be transformed.

5. Materials and methods

5.1. Physicochemical properties determination

5.1.1. Calculation of Mw, HBD, HBA, RtB, and tPSA

Using ACDLAbs PhysChem Suite 14.0 software (Advanced Chemistry Development, Inc., Toronto, ON, Canada), molecular weight, number of hydrogen donors and acceptors, number of rotatable bonds, and polar surface area were calculated.

5.1.2. Dissociation constant determination

pKa values were obtained by spectrophotometric titration on spectrophotometer Agilent Cary-60 (Agilent Technologies, Santa Clara, CA, USA). 20 μL of compound stock solution in DMSO (2 mg/mL) and 20 μL of 0.1 M hydrochloric acid were added into the cuvette with 50% methanol (total volume 3.5 mL). While stirred at 20 °C, the sample was titrated with 0.1 M sodium hydroxide. Absorption spectra (190 – 500 nm) were acquired at different pH values after each base addition. pH values were acquired using pH meter WTW InoLab_IDS Multi 9430 (WTW, Prague, Czech Republic) and pH electrode SenTix® Mic (WTW, Prague, Czech Republic). Absorbance at the chosen wavelength was plotted as a function of pH and the pKa value was determined from the inflection point in the given plot in GraphPadPrism 8.0 software (GraphPad Software, San Diego, CA, USA).

5.1.3. Partition coefficient and distribution coefficient determination

Ten nM sodium phosphate buffer at pH 7.4 was used for logD determination. All solvents were mutually saturated at the temperature of the experiment (21 °C) by the following method: large stock bottles, one containing *n*-octanol and 1 mL of ultrapure water/sodium phosphate buffer, and the other containing ultrapure water/sodium phosphate buffer and 1 mL of *n*-octanol were shaken for 30 min on a mechanical shaker and then left to stand for phases to separate. Approximately 0.50 mg of the tested compound and a 1:1 vol ratio of saturated solvents (250 μL) were added to the test vessels. The test vessels were shaken on a mechanical shaker (Multi Reax, Heidolph Instruments, Schwabach, Germany) for 30 min at the highest speed. Followed by centrifugation (16,873g for 5 min; Eppendorf 5418 Microcentrifuge, Prague, Czech Republic), two phases were separated. The samples from organic and aqueous phases were transferred to separate vials for LC-MS analysis. UHPLC-DAD-MS system (UHPLC Infinity II 1290, detection by DAD and QqQ 6470; Agilent Technologies, Santa Clara, CA, USA), separation on Arion C18 polar column (100 × 2.1 mm, 2.1 μm; Chromservis, Prague, Czech Republic) was subsequently used for determination of exact concentration. The logP/logD values were calculated using the total quantity of substance present in both phases.

5.1.4. Solubility evaluation

Compound solubility determination was performed using nephelometry assays on the NEPHELOstar microplate instrument (BMG Labtech, Offenburg, Germany). Stock solutions of analyzed compounds were prepared in a concentration of 160 μg/mL in ultrapure water and sodium phosphate buffer (pH 7.4), respectively. Each suspension was sonicated at full power with Hielscher UP100H needle ultrasonic processor (Teltow, Germany) to achieve uniform dispersion of particles. Immediately after sonication, the suspension was loaded into NEPHELOstar instrument injector A, together with ultrapure water/sodium phosphate buffer loaded into injector B. Compound dilution was then performed automatically in 48 wells in the range 0–160 μg/mL. After 30 s of shaking, each well was scanned with 80% laser power in matrix 3 × 3, beam width 2 mm. Obtained data were evaluated in GraphPad Prism 7.03 (GraphPad Software, San Diego, CA, USA) using segmental linear regression.

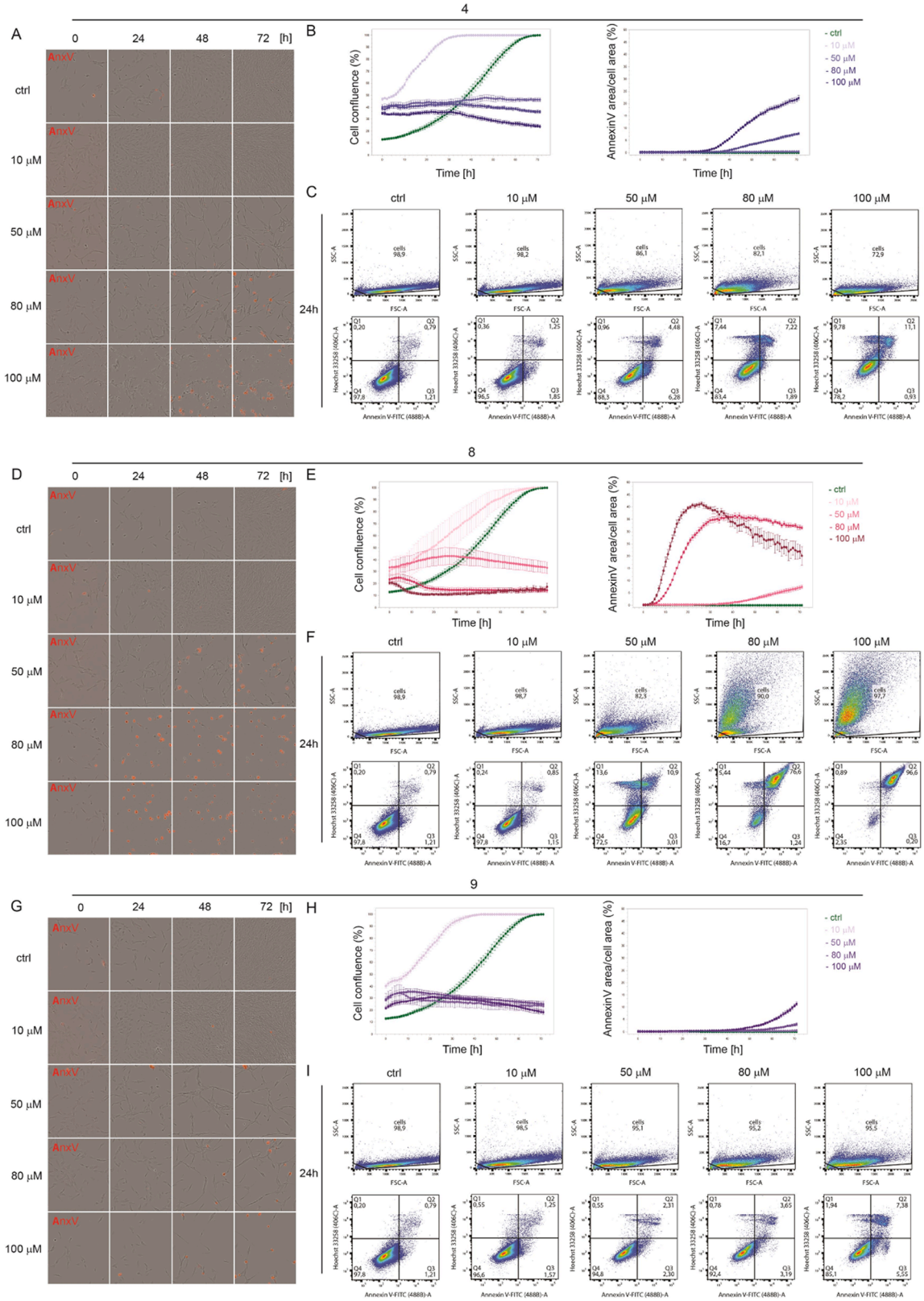

Fig. 9. Apoptosis induced by compounds 4, 8, and 9 in proliferating RPE-1 cells. The cytotoxic effect of compounds **4** (A-C), **8** (D-F), and **9** (G-I) in the concentration range 0 – 100 μM demonstrated by time-lapse microscopy (0 – 72 h) using the Incucyte SX1 platform. The representative regions (566 × 683 μm) of images captured at 0, 24, 48, and 72 h are presented. The red color represents annexin V staining of apoptotic cells. (B, E, H) The graphs plot changes in cell confluence and annexin V staining. Average cell confluence and annexin V staining with standard error from four images are shown. (C, F, I) Apoptosis was detected by fluorescence-activated cell sorting analysis of annexin V/Hoechst 33258 staining (24 h of compound exposure). Upper row plots represent the relative size (FSC) and complexity (SSC) of the cell. Bottom row plots represent annexin V/Hoechst 33258 staining.

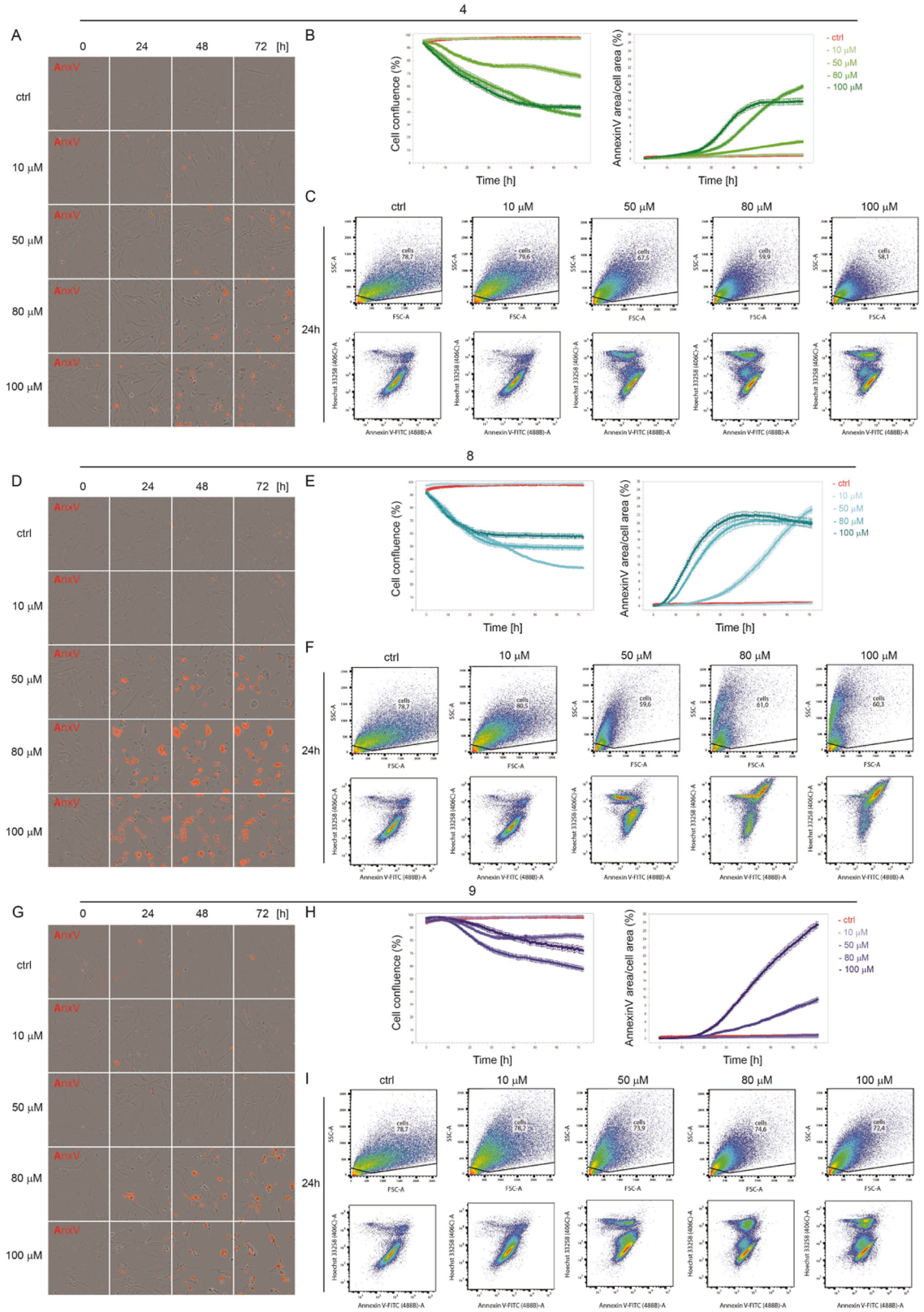

Fig. 10. Apoptosis induced by compounds 4, 8, and 9 in IR-induced senescent RPE-1 cells. (A, D, G) The senolytic effect of compounds in the concentration range 0 – 100 μM demonstrated by time-lapse microscopy (0 – 72 h) using the Incucyte SX1 platform. The representative regions (566 × 683 μm) of images captured at 0, 24, 48, and 72 h are presented. The red color represents annexin V staining of apoptotic cells. (B, E, H) The graphs plot changes in cell confluence and annexin V staining during the treatment. Average cell confluence and annexin V staining with standard error from four images are shown. (C, F, I) Apoptosis was detected by fluorescence-activated cell sorting analysis of annexin V/Hoechst 33258 staining (24 h of compound exposure). Upper row plots represent the relative size (FSC) and complexity (SSC) of the cell. Bottom row plots represent annexin V/Hoechst 33258 staining.

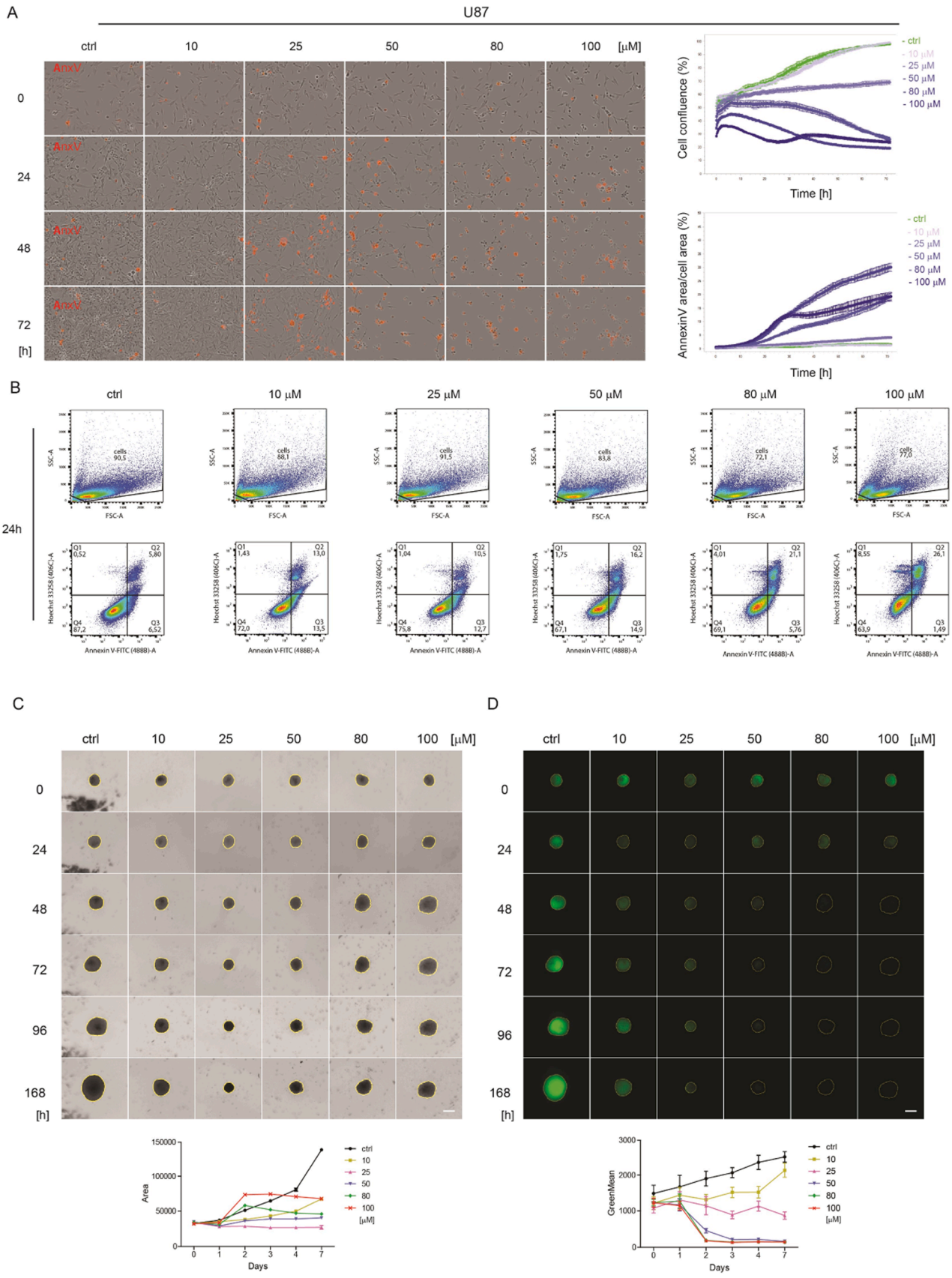

(caption on next page)

Fig. 11. Apoptosis-inducing effect of selected compound 4 on glioblastoma U87 cells. (A) Cytotoxic effect of compound **4** in the concentration range 0 – 100 μM demonstrated by time-lapse microscopy (0 – 72 h) using the Incucyte SX1 platform. The representative regions (707 × 528 μm) of images captured at 0, 24, 48, and 72 h are presented. The red color represents annexin V staining of apoptotic cells. The graphs plot changes in cell confluence and annexin V staining. Average cell confluence and annexin V staining with standard error from four images are shown. (B) Apoptosis was detected by fluorescence-activated cell sorting analysis of annexin V/Hoechst 33258 staining after 24 h of compound **4** exposure. Upper row plots represent the relative size (FSC) and complexity (SSC) of the cell. Bottom row plots represent annexin V/Hoechst 33258 staining. (C) Size and (D) fluorescence (in green) intensity of the 3D spheroids prepared from proliferating U87 cells expressing GFP were detected by ZEISS AxioZoom V.16 microscope. The representative 3D spheroids from six replicates are shown, the scale bar represents 200 μm. The graphs plot changes in the spheroid size and GFP fluorescent intensity (mean ± SD; n = 6).

5.2. In vitro evaluation

5.2.1. Antibodies

For immunoblotting, the following primary and secondary antibodies were used: rabbit polyclonal anti-p70 S6 kinase (#9202), rabbit monoclonal anti-phospho p70 S6 kinase (Thr389) (108D2, #9234) purchased from Cell Signaling Technology, Inc., Danvers MA, USA; mouse monoclonal anti-GAPDH (GTX30666) obtained from GeneTex, Inc., Irvine, CA, USA; and goat anti-mouse (170–6516) or goat anti-rabbit IgG (H + L)-HRP conjugate (170–6515) purchased from Bio-Rad, Hercules, CA, USA.

5.2.2. Cell culture

Human telomerase-immortalized retinal pigment epithelial cells (RPE-1, ATCC® CRL-4000™) were cultured in Dulbecco's modified Eagle's medium (DMEM, Thermo Fisher Scientific, Waltham, MA, USA) with high glucose (4.5 g/L). Primary human skin fibroblasts (BJ, ATCC® CRL-2522™, population doublings 85) were cultured in Dulbecco's modified Eagle's medium (Thermo Fisher Scientific, Waltham, MA, USA) with low glucose (1 g/L). Both cell culture media were supplemented with 10% fetal bovine serum (FBS, Gibco/Thermo Fisher Scientific) and non-essential amino acids (NEAA), 100 units/mL of penicillin, and 100 μg/mL of streptomycin (Sigma-Aldrich). Cells were kept at 37 °C under a 5% CO_2 atmosphere and 95% humidity.

5.2.3. Induction of cellular senescence

To prepare drug-induced senescence (DIS-BJ), BJ cells were exposed to 5 nM docetaxel for 7 days until loss of proliferative activity and development of a senescent phenotype. [46,62,63].

For oncogene-induced senescence (OIS-BJ), BJ fibroblast carrying a tetracycline-regulated ectopic expression of H-RasV12 oncogenic mutant [64,65] were exposed to 2 μg/mL of doxycycline every 48 h for 14 days until loss of proliferative activity and development of senescent phenotype. [63].

To obtain ionizing radiation-induced senescent cells (IR-RPE1), proliferating RPE-1-hTERT cells were exposed to a single dose of 20 Gy using Pantak HF160 (Gulmay, Surrey, UK) X-ray instrument equipped with Pantak Seifert HF320 generator, the MXR-161 X-ray tube (Comet AG, Flamatt, Switzerland), and an aluminum filter using current 1 – 10 mA. After irradiation, the cells were cultured for additional 7 days until the development of a senescent phenotype. [62,63].

To prepare temozolomide (TMZ)-induced senescence, U87 cells were exposed to 100 μM TMZ for 14 days. [62].

The development of cellular senescence was confirmed by the determination of senescence-associated beta-galactosidase activity and detection of DNA replication by 5-ethynyl-2'-deoxyuridine incorporation assays, as we described previously. [62,63].

5.2.4. Crystal violet assay

Crystal violet assay was performed as described previously. [62] Cells were seeded in 96-well plates in densities of 5000 (BJ, A172, T98, U87, TMZ-U87, U373), 3000 (RPE-1), and 2500 (DIS-BJ, OIS-BJ, IR-RPE-1) cells per well. Cells were exposed to compounds in a concentration ranging from 10 to 100 μM for 24 h. Glioblastoma cell lines (A172, T98, U87, U373) were exposed to a combination of compound **4** and temozolomide for 72 h. Then, the cells were washed twice with 150 μL PBS and stained with 30 μL 0.5% w/v crystal violet in 20% methanol for 15 min. Next, the plates were washed 5 times with double-distilled H_2O and left to dry overnight. Crystal violet was solubilized with 75 μL 0.2% Triton X-100 (Sigma) in PBS for 15 min. The absorbance was read at 595 nm using a microplate reader (Multiskan EX, Thermo Electron Corporation). Each condition was carried out at least in triplicate, and absorbance of crystal violet was expressed as a percentage of absorbance of untreated cells. [66].

5.2.5. Resazurin assay

The resazurin reduction assay was performed as described previously. [62] Briefly, cells were seeded onto a 96-well plate and treated with the tested compounds in a concentration range as indicated. After 24 h, 200 μL of the culture medium of each well was exchanged for 100 μL of resazurin (stock 30 mg/mL; Sigma, St. Louis, MO) diluted 10 times in the culture medium, and the cells were incubated at 37 °C for 1 – 3 h. Reading of fluorescence was done using an Envision reader (PerkinElmer, Waltham, MA). Absolute values of fluorescence were related to the values of untreated cells.

5.2.6. Detection of apoptosis by FACS

Adherent cells were harvested by 0.25% trypsin/EDTA, combined with floating cells, collected by centrifugation (1000 rpm, 4 °C, 5 min), resuspended in cold PBS, and again centrifuged. Cell pellets were then resuspended in Annexin V Binding Buffer (ApoFlowEx FITC Kit, ED7044, Exbio, Vestec, Czech Republic). Annexin V-FITC and Hoechst 33258 were added to the cell pellet and mixed. Cells were incubated in the dark at room temperature for 15 min and 100 μL of the sample was analyzed by FACS using the BD FACSVerseTM flow cytometer (BD Biosciences, Franklin Lakes, NJ). Data were analyzed using FlowJo 10 software (FlowJo LLC, Ashland, OR).

5.2.7. Time-lapse microscopy

For auto-monitoring of cells, Incucyte SX1 Live-Cell Analysis System (Sartorius, Göttingen, Germany), located in an incubator maintained at 37 °C under a 5% CO_2 atmosphere and 95% humidity, was utilized. The images (1408 × 1040 pixels at 1.24 μm/pixel) were acquired using a 10 × objective lens in phase contrast, red fluorescence (excitation: 585 ± 20 nm, emission: 635 [625,705] nm, acquisition time: 100 ms) channels every 60 min during 72 h. The first image was acquired 30 min after adding compounds. The images were processed to measure cell confluence using Incucyte software (version 2022 A). Annexin V-Dy647 (Apronex s.r.o., Czech Republic) diluted 1:1500 was used for apoptotic cell staining, annexin V-positive area expressed as a percentage of total cell area is shown in graphs.

5.2.8. Preparation of tumor spheroids and determination of spheroid growth

Cell culture 96-well round-bottom plates were coated with 60 μL/well of polyHEMA (poly(2-hydroxyethyl) methacrylate) diluted in 95% ethanol to obtain a final concentration of 5 mg/mL from the stock solution 120 mg/mL in 95% ethanol. The plates with lids covered were left to dry by evaporation at room temperature inside a sterile hood for 72 h. The 2D cell culture of U87-GFP cells was washed with PBS, and cells detached with 0.25% trypsin/EDTA at 37 °C for 5 min. Two hundred μL of the cell suspension in density 5,000 cell/mL for proliferating U87-GFP: and 25000 cell/mL for senescent U87-GFP was transferred to each well of the 96-well plate pre-coated with polyHEMA (1000 cells per

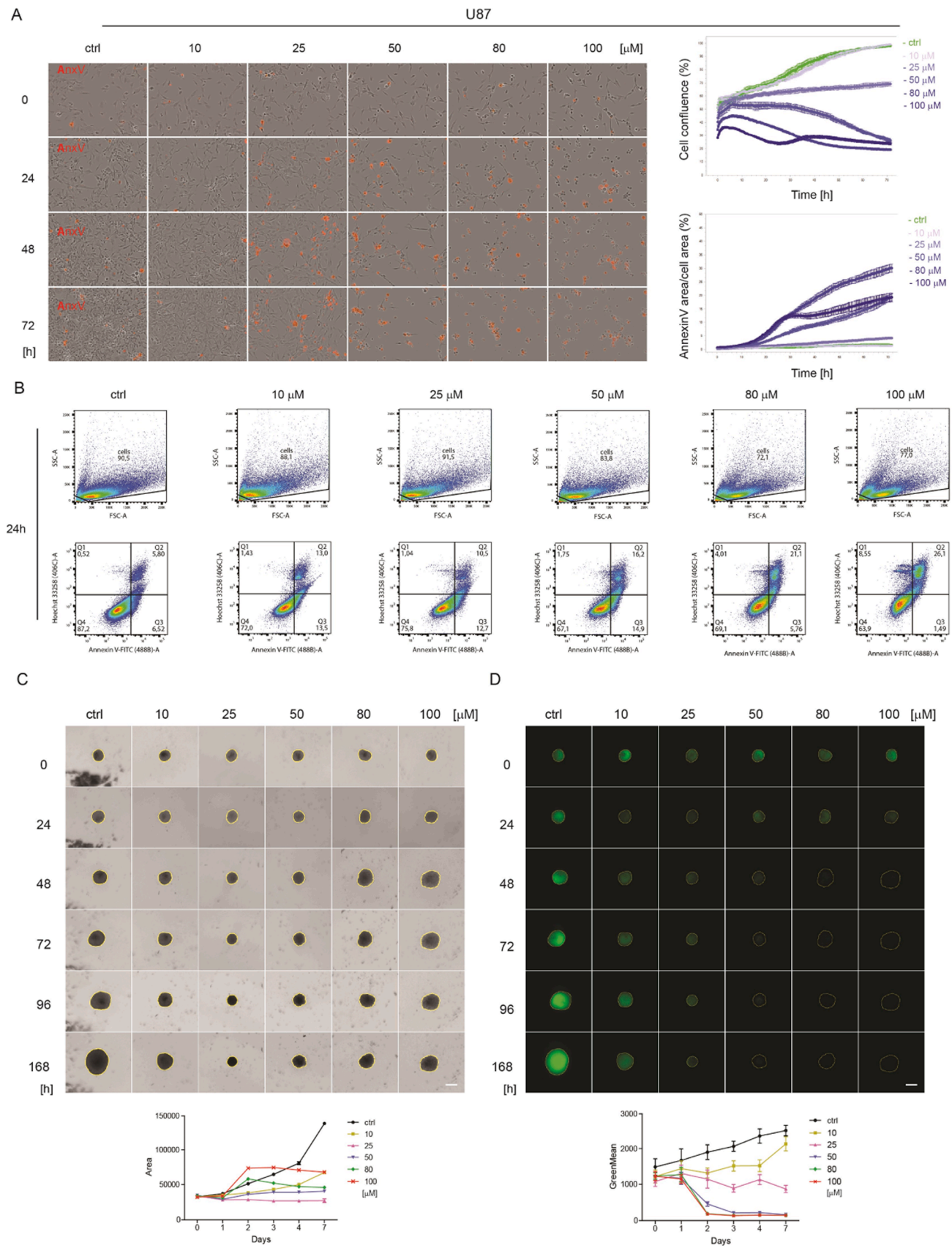

(caption on next page)

Fig. 12. Cell death induced by compound 4 in temozolomide-senescent glioblastoma U87 cells. (A) The senolytic effect of compound **4** (concentration range of 0 – 100 μM) was demonstrated by time-lapse microscopy (0 – 72 h) using the Incucyte SX1 platform. The representative regions (707 × 528 μm) of images captured at 0, 24, 48, and 72 h are presented. The red color represents annexin V staining of apoptotic cells. The graphs plot changes in cell confluence and annexin V staining. Average cell confluence and annexin V staining with standard error from four images are shown. (B) Apoptosis was detected by fluorescence-activated cell sorting analysis of annexin V/Hoechst 33258 staining after 24 h of compound **4** exposure. Upper row plots represent the relative size (FSC) and complexity (SSC) of the cell. Bottom row plots represent annexin V/Hoechst 33258 staining. (C) Size and (D) fluorescence green intensity of the 3D spheroids prepared from TMZ-induced (100 μM, 14 days) senescent U87 cells expressing GFP were detected by ZEISS AxioZoom V.16 microscope, the scale bar represents 200 μm. The representative 3D spheroids from six replicates are shown. The graphs plot changes in the spheroid size and GFP fluorescent intensity (mean ± SD; n = 6).

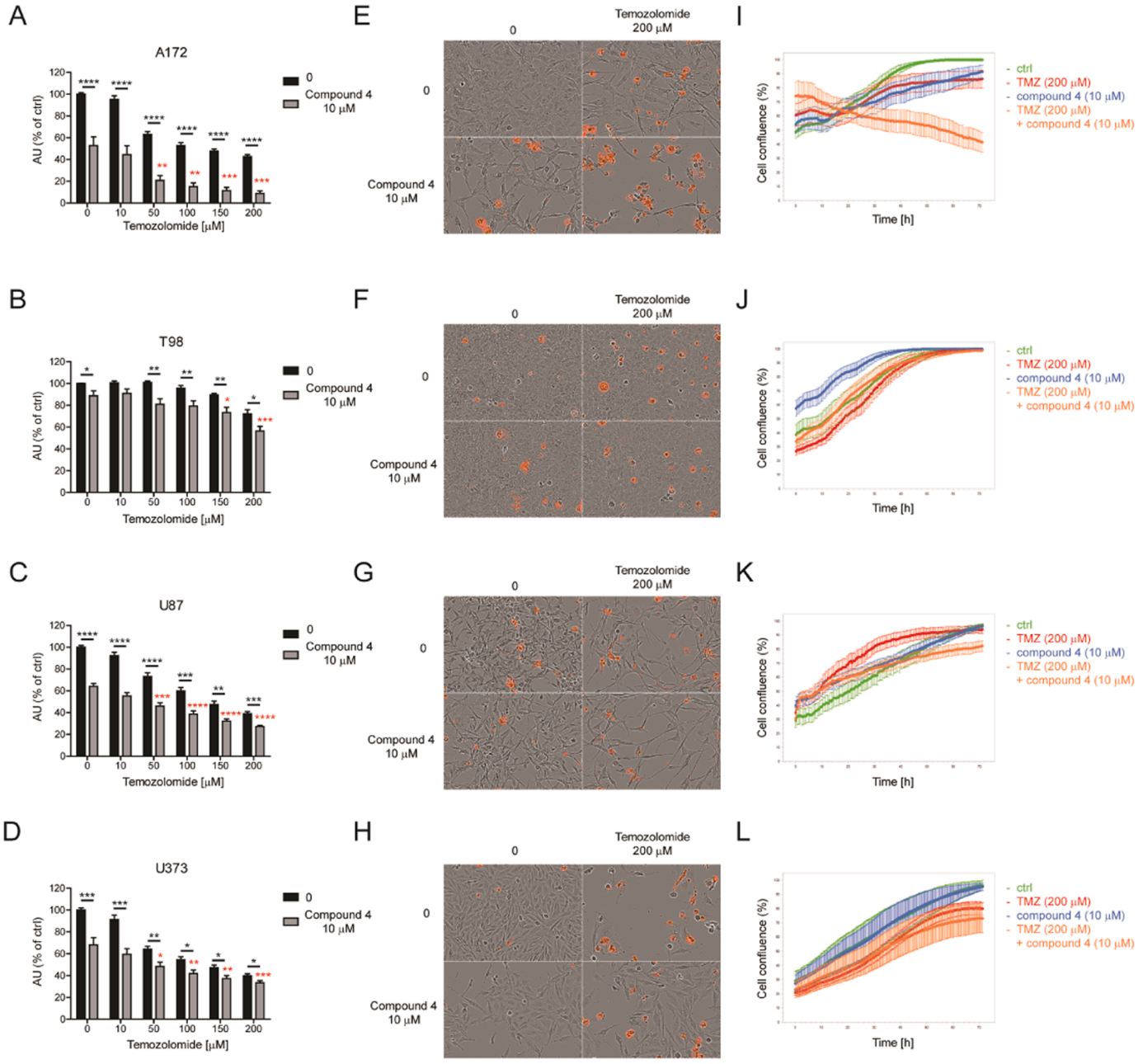

Fig. 13. Synergic effect of compounds 4 and temozolomide on survival of glioblastoma A172, T98, U87, and U373 cells. (A, B, C, D) The cytotoxic effect of compound **4** (concentration range of 0 – 100 μM) with temozolomide (concentration range of 0 – 200 μM) was detected by crystal violet staining (72 h). The experiment was done in duplicate. Data were normalized to untreated cells and plotted as mean ± SEM. Student's t-test, * ** *, $p < 0.0001$; * ** , $p < 0.001$; * *, $p < 0.01$; * , $p < 0.05$. Black stars indicate conditions where the effect of drug combination was significantly more affected than by temozolomide alone. Red stars indicate conditions where the drug combination effect is significantly more affected than compound **4** alone. (E, F, G, H) The cytotoxic effect was demonstrated by time-lapse microscopy (0 – 72 h) using the Incucyte SX1 platform. The representative regions (606 × 429 μm) of images were captured at 72 h. The red color represents annexin V staining of apoptotic cells. (I, J, K, L) The graphs plot changes in cell confluence during the treatment. Average cell confluence with standard error from four images is shown.

Table 4
Effect of **4** on 24 h of survival in mice.

Dose (mg/kg i. p.)	Total number dead/treated		LD_{50} (95% confidence limit) (mg/kg)	
	Male	Female	Male	Female
375.0	0/8	0/8	559.02 (511.36 – 611.11)	575.52 (534.07 – 620.19)
500.0	2/8	1/8		
625.0	6/8	6/8		
750.0	8/8	8/8		

LD_{50} was calculated according to Litchfield & Wilcoxon.

Table 5
Effect of **8** on 24 h of survival in mice.

Dose (mg/kg i. p.)	Total number dead/treated		LD_{50} (95% confidence limit) (mg/kg)	
	Male	Female	Male	Female
250.0	2/8	1/8	360.59 (289.35 – 449.36)	478.63 (393.96 – 581.51)
375.0	4/8	2/8		
500.0	6/8	4/8		
750.0	8/8	8/8		

LD_{50} was calculated according to Litchfield & Wilcoxon.

Table 6
Effect of **9** on 24 h of survival in rats and mice.

Dose (mg/kg i. p.)	Total number dead/treated		LD_{50} (95% confidence limit) (mg/kg)	
	Male	Female	Male	Female
375.0	2/8	0/8	489.37 (416.04 – 575.62)	500.0 (432.80 – 577.63)
500.0	4/8	4/8		
625.0	6/8	6/8		
750.0	8/8	8/8		

LD_{50} was calculated according to Litchfield & Wilcoxon.

spheroid/well). To form the spheroids, the plate was centrifuged at 200g at room temperature for 5 min and then incubated on a rotary shaker in the cell culture incubator at 37 °C, 5% CO_2 for 3 days. Three days after the seeding, 100 μL of the conditioned medium was changed with a fresh medium with two times concentrated compound 4 (10 mM stock solution).

The spheroid growth and size were followed daily by scanning bright-field and fluorescence for 5 days, and also at day 7 post-treatment using ZEISS AxioZoom V.16 microscope equipped with PlanNeoFluar Z 1.0 × /0.25 objective and eGFP Filter set 38 HE (each spheroid in a hexaplicate). Images were analyzed using Fiji distribution of ImageJ [67] and made-to-measure macros. The fold change of the total green fluorescence to the starting time point was plotted.

5.2.9. SDS-PAGE and immunoblotting

Cells were washed three times with PBS, harvested into 95 °C heated SDS sample lysis buffer (2% SDS, 50 mM Tris–Cl, pH 6.8, 10% glycerol in double-distilled H_2O), and sonicated at 3 μm amplitude for 3 × 30 s with 30 s cooling intervals in a Diagenode Bioruptor 300 (Diagenode, Liege, Belgium) for human cell lines. The concentration of proteins was estimated by the PierceTM BCA Protein Assay (Thermo Scientific, Waltham, MA). DTT (100 mM) and 0.01% bromophenol blue were added to the lysates before separation by SDS-PAGE (10% gels were used). Equal protein amounts (40 μg) were loaded into each well. Proteins were electrotransferred onto a nitrocellulose membrane (AmershamTM ProtranTM 0.45 mm NC, GE Healthcare, Chalfont St Giles, UK) using wet transfer and detected by specific antibodies (at 4 °C overnight) combined with HRP-conjugated secondary antibodies. Peroxidase activity was detected by AmershamTM ECL Western Blotting Detection Reagents (GE Healthcare, Chalfont St Giles, UK). GAPDH was used as a loading control. Quantitative analysis of immunoblots was done by ImageJ 1.48 v program [68] with GAPDH as the internal control.

5.2.10. Determination of cytokine expression and secretion

All 10 compounds were tested for their effect on the production of 11 proinflammatory cytokines into cell culture media conditioned by IR-induced senescent RPE-1 cells, which were cultivated on 12-well plates at a density of 32,000 cells per well. Compounds **1** – **7** were tested at 100 μM concentration which had no or insignificant effect on the number of senescent cells. Compound **9** was used at 80 μM, and compound **8** was used at 50 μM concentrations. After 24 h exposure of cell cultures to compounds, the culture medium was removed, cells were washed three times with 1 mL PBS, and a fresh medium without FBS was added for another 24 h. Detection of cytokines in conditioned media was done by Human Inflammation 11-Plex Panel: (IFNγ, IL-1α, IL-1β, IL-6, IL-8, IL-10, IL-12p70, IL-27, IP-10, MCP-1, and TNFα) (AimPlex Biosciences, Inc.) using a BD FACSVerseTM flow cytometer (BD Biosciences, Franklin Lakes, NJ) according to manufacturer's protocol. Data were analyzed using FlowJo 10 software (FlowJo LLC, Ashland, OR).

5.2.11. Statistics

Graphs and statistics in the figures were generated using GraphPad Prism 5, Version 5.04 (GraphPad Software, Inc., La Jolla, CA).

5.3. In vivo experiments

5.3.1. Experimental animals

This study was performed on adult outbred albino male male and female Swiss mice 10 – 12 weeks old, weighing 24 – 28 g, respectively (Veterinary Service Center, Military Health Care Department, Belgrade, Serbia). The experimental animals were housed in plastic cages (Macrolon® cage type 4, Bioscape, Germany) with sawdust bedding (Versele-Laga, Belgium) certificated as having contaminant levels below toxic concentrations. The environmental conditions were controlled and monitored by a central computer-assisted system with a temperature of 22 ± 2 °C, relative humidity of 55 ± 15%, 15 – 20 air changes/h, and artificial lighting of approximately 220 lux (12 hrs light/dark cycle). The experimental animals had free access to food, commercial pellets for mice (Gebi, Čantavir, Serbia), and tap water from municipal mains, filtered through a 1.0 μm filter (Skala Green, Serbia).

All animal care and experimental procedures were approved by the Ethical Commission for the Protection of Animal Welfare, Faculty of Veterinary Medicine, University of Belgrade, Serbia (opinion 12/2021, decision No.: 01–442/1 from 27.05.2021), which was confirmed by the Ethical Committee of the Veterinary Directorate, Ministry of Agriculture, Forestry and Water Management, Belgrade, Serbia (decision No. 323–07–06024/2021–05 from 10.06.2021).

5.3.2. Determination of intraperitoneal median lethal dose of 4, 8, and 9 in mice

The median lethal dose (LD_{50}) of **4**, **8**, and **9** was established by using four groups of male and female mice, respectively. Experimental groups consisted of 8 animals each. Increasing doses of each compound were applied by intraperitoneal (i.p.) route in a separate group of mice, both genders, as presented in Table S1 (SI). Intraperitoneal administration of **4**, **8**, and **9** was carried out in the lower right quadrant of the abdomen towards the head at a 30 – 40° angle horizontal to avoid damage to the urinary bladder, cecum and other abdominal organs. The selection of dose levels for the determination of intramuscular LD_{50} was based on the experimental protocol published earlier. [60,61] For evaluation of dose-depend acute toxicity, four dose groups of mice of both genders were included: a low-dose group (a dose that produces no compound-related toxicity); a mid-dose group (a dose that elicits some minimal signs of compound-induced toxicity); a high-dose group (a dose that results in prominent compound-induced toxic effects); and a highest-dose group (a dose that results in the death of all treated

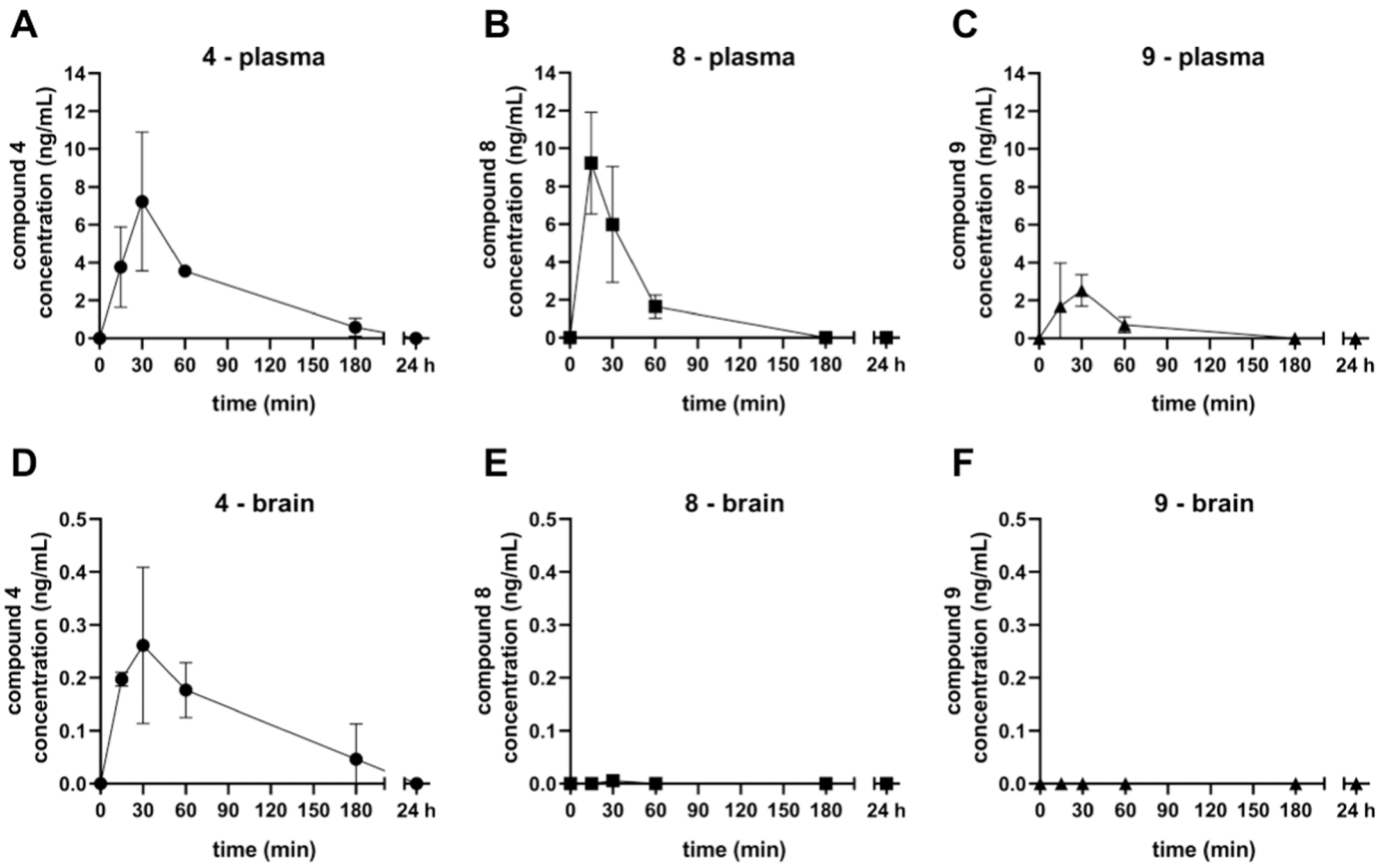

Fig. 14. The pharmacokinetics of **4**, **8**, and **9**. The graphs show the changes in the concentrations of the studied compounds **4**, **8**, and **9** over time in the mouse plasma (A, B, and C, respectively) and brain tissue (D, E, and F, respectively) after i.p. administration of the 1 mg/kg dose. Data are shown as mean ± S.D., n = 3 per time point.

animals).

5.3.3. The general condition of the experimental animals

After treatment, all animals were observed for the 2, 4, 6, 24, 72, 96 h, 7 and 14 days for any toxic symptoms. Then, their general condition was observed daily throughout the whole experiment, lasting 14 days.

5.3.4. Median lethal dose

After 24 h, all dead animals were counted, and the median lethal dose (LD_{50}) for **4**, **8**, and **9** was calculated according to the method of Litchfield & Wilcoxon. [69].

5.3.5. Pharmacokinetic study

Forty-eight male C57BL/6 mice (8 months, 28 – 36 g, Envigo) were used. The mice were single-housed in transparent plastic individually ventilated cages (32 × 17 × 12 cm) in an animal room of the National Institute of Mental Health, Klecany, Czech Republic, with constant temperature (22 °C), humidity (40 – 70%), a 12 h light/dark cycle and with water and food available *ad libitum*. The experiments were conducted in accordance with the guidelines of European Union directive 2010/63/EU and Act No. 246/1992 Coll. on the protection of animals against cruelty, and were approved by the Animal Care and Use Committee of the National Institute of Mental Health (reference number MZDR 22468/2021–5/OVZ).

The mice were intraperitoneally injected with the compounds **4**, **8**, or **9** dissolved in 1% Tween 80 (Fisher Chemical, UK) in physiological saline. The dose was 1 mg/kg (injection volume 10 mL/kg). The mice were sacrificed 15, 30, 60, 180 min, and 24 h after drug administration (3 mice for each drug and time interval). Three animals were used as blank controls. The mice were anesthetized in isoflurane (Forane, AbbVie, Czech Republic) inhalation anesthesia, decapitated, and blood and brains were collected. Blood was collected in K_3EDTA tubes, centrifuged, and plasma was collected and stored at − 80 °C. Brains were weighed, frozen on dry ice, and stored at − 80 °C prior to sample preparation and analysis.

Frozen brains were homogenized in 1 mL of cold PBS using the Fastprep-24 5 G sample disruption instrument. Thawed plasma or homogenized brain in the volume of 100 μL, was mixed with the same volume of methanol and acetonitrile, vortexed for 15 min, and centrifuged at 14000g for 3 min. The supernatant was then filtered through a 0.22 μm PTFE syringe filter into the vial and measured.

Detection of **4**, **8**, and **9** was performed on the Agilent 1290 Infinity II UHPLC system coupled to the Agilent 6470 QqQ mass spectrometer. Chromatographic conditions were maintained at gradient elution of 0.4 mL/min by 0.1% formic acid in water and acetonitrile (0–0.5 50:50, 0.5–3.0 gradient to 5:95, 3.0–4.0 5:95, 4.0–5.0 50:50), thermostated autosampler set to 15 °C and column thermostat equipped with the Zorbax Eclipse plus RRHD C18 2.1 × 50 mm, 1.8 μm (PN 959757–902) column kept to 30 °C. MS source parameters were set to the following: drying gas 200 °C at 8 L/min, sheath gas 400 °C at 12 L/min, nebulizer pressure 40 psi, capillary voltage 2500 V and nozzle voltage 300 V. **4** transitions of $[M+H]^+$ ions *m/z* were detected with the setting of dwell time 60 ms, cell accelerator 4 V, fragmentor 146 V for 438→235, 208 and 166 (collision energy – CE 32, 60 and 60 V). **8** transitions of $[M+H]^+$ ions *m/z* were detected with the setting of dwell time 60 ms, cell accelerator 4 V, fragmentor 137 V for 400→235, 166 and 138 (CE 24, 60 and 60 V). **9** transitions of $[M+H]^+$ ions *m/z* were detected with setting of dwell time 60 ms, cell accelerator 4 V, fragmentor 129 V for 365→196 and 150 (CE 16 and 48 V). The data (plasma and brain

concentrations of the compounds over time) were plotted on a graph as mean ± S.D. using GraphPad Prism 8 (San Diego, USA).

CRediT authorship contribution statement

Zofia Chrienova: Manuscript writing, Chemical synthesis, Physical-chemical properties determination; **David Rysanek:** Manuscript writing, Cytotoxicity assays; **Josef Novak:** Time-lapse microscopy; **Pavla Vasicova:** *in vitro* experiments, **Patrik Oleksak:** Chemical synthesis; **Rudolf Andrys:** Physical-chemical properties determination; **Adam Skarka:** Solubility determination, Pharmacokinetic analysis; **Jelena Dumanovic, Zoran Milovanovic, Vesna Jacevic:** Acute toxicity experiment; **Marketa Chvojkova, Kristina Holubova, Karel Vales:** Pharmacokinetic study; **Veronika Skoupilova:** *In vitro* experiments; **Marian Valko, Klaudia Jomova, Suliman Y. Alomar:** Conceptualization, Manuscript editing; **Fernanda D. Botelho, Tanos C. C., Franca:** *in silico* study; **Kamil Kuca:** Manuscript editing; **Zdenek Hodny:** Manuscript writing, Supervision, Conceptualization; **Eugenie Nepovimova:** Manuscript writing, Supervision, Conceptualization.

Declaration of Competing Interest

The authors declare no conflict of interest.

Acknowledgments

This work was supported by the Ministry of Health of the Czech Republic (No. NV19–09-00578), the University of Hradec Kralove (Faculty of Science, no. 2108–2023), and the Institutional Grant (project RVO 68378050). ZH, PV, and DR were supported by the project National Institute for Cancer Research (Programme EXCELES, ID Project No. LX22NPO5102) – Funded by the European Union – Next Generation EU. MC, KH and KV were partially supported by the project National Institute for Neurological Research (Programme EXCELES, ID Project No. LX22NPO5107 – MEYS) – Funded by the European Union – Next Generation EU. MV and KJ were supported by the Slovak Scientific Grant Agencies (VEGA 1/0482/20 and APVV-19–0087). The authors would like to thank the Researchers Supporting Project (number RSP2023R35), King Saud University, Riyadh, Saudi Arabia. The Medical Faculty of the Military Medical Academy, University of Defence in Belgrade, Serbia (MFVMA01/23–25) partially supported this work. Additionally, the authors would like to express their gratitude to Prof. Kamil Musilek and Dr. Ondrej Benek for providing the substances as well as to Marketa Vancurova for her excellent technical support.

Appendix A. Supporting information

Supplementary data associated with this article can be found in the online version at doi:10.1016/j.biopha.2023.115600.

References

[1] J. Martel, D.M. Ojcius, C.-Y. Wu, H.-H. Peng, L. Voisin, J.-L. Perfettini, Y.-F. Ko, J. D. Young, Emerging use of senolytics and senomorphics against aging and chronic diseases, Med. Res. Rev. 40 (6) (2020) 2114–2131, https://doi.org/10.1002/med.21702.

[2] M. Borghesan, W.M.H. Hoogaars, M. Varela-Eirin, N. Talma, M. Demaria, A senescence-centric view of aging: implications for longevity and disease, Trends Cell Biol. 30 (10) (2020) 777–791, https://doi.org/10.1016/j.tcb.2020.07.002.

[3] M. Collado, M.A. Blasco, M. Serrano, Cellular senescence in cancer and aging, Cell 130 (2) (2007) 223–233, https://doi.org/10.1016/j.cell.2007.07.003.

[4] B.G. Childs, M. Durik, D.J. Baker, J.M. van Deursen, Cellular senescence in aging and age-related disease: from mechanisms to therapy, Nat. Med. 21 (12) (2015) 1424–1435, https://doi.org/10.1038/nm.4000.

[5] S. Saez-Atienzar, E. Masliah, Cellular senescence and alzheimer disease: the egg and the chicken scenario, Nat. Rev. Neurosci. 21 (8) (2020) 433–444, https://doi.org/10.1038/s41583-020-0325-z.

[6] D. Muñoz-Espín, M. Serrano, Cellular senescence: from physiology to pathology, Nat. Rev. Mol. Cell Biol. 15 (7) (2014) 482–496, https://doi.org/10.1038/nrm3823.

[7] M.V. Blagosklonny, Disease or not, aging is easily treatable, Aging 10 (11) (2018) 3067–3078, https://doi.org/10.18632/aging.101647.

[8] M.V. Blagosklonny, Validation of anti-aging drugs by treating age-related diseases, Aging 1 (3) (2009) 281–288, https://doi.org/10.18632/aging.100034.

[9] M.V. Blagosklonny, Koschei the immortal and anti-aging drugs, Cell Death Dis. 5 (2014), e1552, https://doi.org/10.1038/cddis.2014.520.

[10] D. Gems, What is an anti-aging treatment? Exp. Gerontol. 58 (2014) 14–18, https://doi.org/10.1016/j.exger.2014.07.003.

[11] E.J. Brown, M.W. Albers, T.B. Shin, K. Ichikawa, C.T. Keith, W.S. Lane, S. L. Schreiber, A mammalian protein targeted by g1-arresting rapamycin-receptor complex, Nature 369 (6483) (1994) 756–758, https://doi.org/10.1038/369756a0.

[12] Z. Chrienova, E. Nepovimova, K. Kuca, The role of MTOR in age-related diseases, J. Enzym. Inhib. Med. Chem. 36 (1) (2021) 1679–1693, https://doi.org/10.1080/14756366.2021.1955873.

[13] T. Vellai, K. Takacs-Vellai, Y. Zhang, A.L. Kovacs, L. Orosz, F. Müller, Genetics: influence of TOR kinase on lifespan in C. elegans, Nature 426 (6967) (2003) 620, https://doi.org/10.1038/426620a.

[14] D.E. Harrison, R. Strong, Z.D. Sharp, J.F. Nelson, C.M. Astle, K. Flurkey, N. L. Nadon, J.E. Wilkinson, K. Frenkel, C.S. Carter, M. Pahor, M.A. Javors, E. Fernandez, R.A. Miller, Rapamycin fed late in life extends lifespan in genetically heterogeneous mice, Nature 460 (7253) (2009) 392–395, https://doi.org/10.1038/nature08221.

[15] D.D. Sarbassov, S.M. Ali, D.M. Sabatini, Growing roles for the MTOR pathway, Curr. Opin. Cell Biol. 17 (6) (2005) 596–603, https://doi.org/10.1016/j.ceb.2005.09.009.

[16] S. Wullschleger, R. Loewith, M.N. Hall, TOR signaling in growth and metabolism, Cell 124 (3) (2006) 471–484, https://doi.org/10.1016/j.cell.2006.01.016.

[17] M.V. Blagosklonny, Aging: ROS or TOR, Cell Cycle Georget. Tex. 7 (21) (2008) 3344–3354, https://doi.org/10.4161/cc.7.21.6965.

[18] Y. Wei, Y.-J. Zhang, Y. Cai, M.-H. Xu, The role of mitochondria in MTOR-regulated longevity, Biol. Rev. Camb. Philos. Soc. 90 (1) (2015) 167–181, https://doi.org/10.1111/brv.12103.

[19] Y. Wei, Y.-J. Zhang, Y. Cai, Growth or longevity: the TOR's decision on lifespan regulation, Biogerontology 14 (4) (2013) 353–363, https://doi.org/10.1007/s10522-013-9435-6.

[20] T. Weichhart, MTOR as regulator of lifespan, aging, and cellular senescence: a mini-review, Gerontology 64 (2) (2018) 127–134, https://doi.org/10.1159/000484629.

[21] I. Afanas'ev, Signaling and damaging functions of free radicals in aging-free radical theory, hormesis, and TOR, Aging Dis. 1 (2) (2010) 75–88.

[22] D.A. Butterfield, B. Halliwell, Oxidative stress, dysfunctional glucose metabolism and Alzheimer disease, Nat. Rev. Neurosci. 20 (3) (2019) 148–160, https://doi.org/10.1038/s41583-019-0132-6.

[23] K. El Hadri, R. Smith, E. Duplus, C. El Amri, Inflammation, oxidative stress, senescence in atherosclerosis: thioredoxine-1 as an emerging therapeutic target, Int. J. Mol. Sci. 23 (1) (2021) 77, https://doi.org/10.3390/ijms23010077.

[24] S.D. Yan, D.M. Stern, Mitochondrial dysfunction and Alzheimer's disease: role of amyloid-beta peptide alcohol dehydrogenase (ABAD), Int. J. Exp. Pathol. 86 (3) (2005) 161–171, https://doi.org/10.1111/j.0959-9673.2005.00427.x.

[25] S.R. Steinhubl, Why have antioxidants failed in clinical trials?, ^{14}D–^{19}D, Am. J. Cardiol. 101 (10A) (2008), https://doi.org/10.1016/j.amjcard.2008.02.003.

[26] Walker, S.E.; Solsky, M.; Schnitzer, B. Prolonged lifespans in female NZB/NZW mice treated with the experimental immunoregulatory drug frentizole. Arthritis and rheumatism. ⟨https://doi.org/10.1002/art.1780251104⟩.

[27] Hatfield, S.M.; Hartley, L.W.; Schmidtke, J.R. The immunomodulatory action of frentizole, a novel immunosuppressive agent. Immunopharmacology. ⟨https://doi.org/10.1016/0162–3109(82)90047–9⟩.

[28] Scheetz, M.E.; Carlson, D.G.; Schinitsky, M.R. Frentizole, a novel immunosuppressive, and azathioprine: their comparative effects on host resistance to Pseudomonas aeruginosa, Candida albicans, herpes simplex virus, and influenza (Ann Arbor) virus. Infection and immunity. ⟨https://doi.org/10.1128/iai.15.1.145–148.1977⟩.

[29] Xie, Y.; Deng, S.; Chen, Z.; Yan, S.; Landry, L. Identification of small-molecule inhibitors of the Abeta-ABAD interaction. Bioorganic & medicinal chemistry letters. ⟨https://doi.org/10.1016/j.bmcl.2006.05.099⟩.

[30] L. Aitken, O. Benek, B.E. McKelvie, R.E. Hughes, L. Hroch, M. Schmidt, L.L. Major, L. Vinklarova, K. Kuca, T.K. Smith, K. Musilek, F.J. Gunn-Moore, Novel benzothiazole-based ureas as 17β-HSD10 inhibitors, a potential Alzheimer's disease treatment, E2757, Mol. Basel Switz. 24 (15) (2019), https://doi.org/10.3390/molecules24152757.

[31] M. Schmidt, O. Benek, L. Vinklarova, M. Hrabinova, L. Zemanova, M. Chribek, V. Kralova, L. Hroch, R. Dolezal, A. Lycka, L. Prchal, D. Jun, L. Aitken, F. Gunn-Moore, K. Kuca, K. Musilek, Benzothiazolyl ureas are low micromolar and uncompetitive inhibitors of 17β-HSD10 with Implications to Alzheimer's disease treatment, E2059, Int. J. Mol. Sci. 21 (6) (2020), https://doi.org/10.3390/ijms21062059.

[32] L. Hroch, O. Benek, P. Guest, L. Aitken, O. Soukup, J. Janockova, K. Musil, V. Dohnal, R. Dolezal, K. Kuca, T.K. Smith, F. Gunn-Moore, K. Musilek, Design, synthesis and in vitro evaluation of benzothiazole-based ureas as potential ABAD/17β-HSD10 modulators for Alzheimer's disease treatment, Bioorg. Med. Chem. Lett. 26 (15) (2016) 3675–3678, https://doi.org/10.1016/j.bmcl.2016.05.087.

[33] L. Hroch, P. Guest, O. Benek, O. Soukup, J. Janockova, R. Dolezal, K. Kuca, L. Aitken, T.K. Smith, F. Gunn-Moore, D. Zala, R.R. Ramsay, K. Musilek, Synthesis and evaluation of frentizole-based indolyl thiourea analogues as MAO/ABAD inhibitors for Alzheimer's disease treatment, Bioorg. Med. Chem. 25 (3) (2017) 1143–1152, https://doi.org/10.1016/j.bmc.2016.12.029.

[34] O. Benek, L. Hroch, L. Aitken, R. Dolezal, P. Guest, M. Benkova, O. Soukup, K. Musil, K. Kuca, T.K. Smith, F. Gunn-Moore, K. Musilek, 6-benzothiazolyl ureas, thioureas and guanidines are potent inhibitors of ABAD/17β-HSD10 and potential drugs for Alzheimer's disease treatment: design, synthesis and in vitro evaluation, Med. Chem. Shariqah U. Arab Emir. (2017).
[35] O. Benek, L. Hroch, L. Aitken, F. Gunn-Moore, L. Vinklarova, K. Kuca, D.I. Perez, C. Perez, A. Martinez, Z. Fisar, K. Musilek, 1-(Benzo[d]Thiazol-2-Yl)-3-phenylureas as dual inhibitors of casein kinase 1 and ABAD enzymes for treatment of neurodegenerative disorders, J. Enzym. Inhib. Med. Chem. 33 (1) (2018) 665–670, https://doi.org/10.1080/14756366.2018.1445736.
[36] F.D. Botelho, E. Nepovimova, K. Kamil, T.C.C. Franca, Virtual screening and molecular dynamic study of potential new binders to MTOR, J. Mol. Model. 28 (10) (2022), 315, https://doi.org/10.1007/s00894-022-05309-2.
[37] H.-Y. Qiu, P.-F. Wang, M. Zhang, A patent review of MTOR inhibitors for cancer therapy (2011-2020), Expert Opin. Ther. Pat. 31 (11) (2021) 965–975, https://doi.org/10.1080/13543776.2021.1940137.
[38] P. Oleksak, E. Nepovimova, Z. Chrienova, K. Musilek, J. Patocka, K. Kuca, Contemporary MTOR inhibitor scaffolds to diseases breakdown: a patent review (2015-2021), Eur. J. Med. Chem. 238 (2022), 114498, https://doi.org/10.1016/j.ejmech.2022.114498.
[39] B. Mao, Q. Zhang, L. Ma, D.-S. Zhao, P. Zhao, P. Yan, Overview of research into MTOR inhibitors, Mol. Basel Switz. 27 (16) (2022) 5295, https://doi.org/10.3390/molecules27165295.
[40] Lipinski, C.A.; Lombardo, F.; Dominy, B.W.; Feeney, P.J. Experimental and Computational Approaches to Estimate Solubility and Permeability in Drug Discovery and Development Settings1PII of Original Article: S0169–409X(96) 00423–1. The Article Was Originally Published in Advanced Drug Delivery Reviews 23 (1997) 3–25.1. *Adv. Drug Deliv. Rev.* 2001, 46 (1), 3–26. https://doi.org/10.1016/S0169–409X(00)00129–0.
[41] D.F. Veber, S.R. Johnson, H.-Y. Cheng, B.R. Smith, K.W. Ward, K.D. Kopple, Molecular properties that influence the oral bioavailability of drug candidates, J. Med. Chem. 45 (12) (2002) 2615–2623, https://doi.org/10.1021/jm020017n.
[42] R. Bhat, E.P. Crowe, A. Bitto, M. Moh, C.D. Katsetos, F.U. Garcia, F.B. Johnson, J. Q. Trojanowski, C. Sell, C. Torres, Astrocyte senescence as a component of Alzheimer's disease, PloS One 7 (9) (2012), e45069, https://doi.org/10.1371/journal.pone.0045069.
[43] D. Sk, W. J, S. E, B. E, A. F, F. B, W. B, B. Re, O. Tc, Z. Y, A. Ps, C. M, S. Ph, X. P, W. M, Z. B, Z. H, O. Me, Profiling senescent cells in human brains reveals neurons with CDKN2D/P19 and tau neuropathology, Nat. Aging 1 (12) (2021), https://doi.org/10.1038/s43587-021-00142-3.
[44] S. Ak, K. M, U. R, M. Ln, Emerging anti-aging strategies - scientific basis and efficacy, Aging Dis. 9 (6) (2018), https://doi.org/10.14336/AD.2018.1026.
[45] V. Myrianthopoulos, K. Evangelou, P.V.S. Vasileiou, T. Cooks, T. P. Vassilakopoulos, G.A. Pangalis, M. Kouloukoussa, C. Kittas, A.G. Georgakilas, V. G. Gorgoulis, Senescence and senotherapeutics: a new field in cancer therapy, Pharmacol. Ther. 193 (2019) 31–49, https://doi.org/10.1016/j.pharmthera.2018.08.006.
[46] O. Sapega, R. Mikyšková, J. Bieblová, B. Mrázková, Z. Hodný, M. Reiniš, Distinct phenotypes and "bystander" effects of senescent tumour cells induced by docetaxel or immunomodulatory cytokines, Int. J. Oncol. 53 (5) (2018) 1997–2009, https://doi.org/10.3892/ijo.2018.4553.
[47] N. Herranz, S. Gallage, M. Mellone, T. Wuestefeld, S. Klotz, C.J. Hanley, S. Raguz, J.C. Acosta, A.J. Innes, A. Banito, A. Georgilis, A. Montoya, K. Wolter, G. Dharmalingam, P. Faull, T. Carroll, J.P. Martínez-Barbera, P. Cutillas, F. Reisinger, M. Heikenwalder, R.A. Miller, D. Withers, L. Zender, G.J. Thomas, J. Gil, MTOR regulates MAPKAPK2 translation to control the senescence-associated secretory phenotype, Nat. Cell Biol. 17 (9) (2015) 1205–1217, https://doi.org/10.1038/ncb3225.
[48] D.E. Johnson, R.A. O'Keefe, J.R. Grandis, Targeting the IL-6/JAK/STAT3 signalling axis in cancer, Nat. Rev. Clin. Oncol. 15 (4) (2018) 234–248, https://doi.org/10.1038/nrclinonc.2018.8.
[49] L. Wang, J. Lan, J. Tang, N. Luo, MCP-1 targeting: shutting off an engine for tumor development, Oncol. Lett. 23 (1) (2022), 26, https://doi.org/10.3892/ol.2021.13144.
[50] M. Epelbaum, [Visual development in the child. The stages], Soins. Gynecol. Obstet. Pueric. Pediatr. No. 120 (1991) 7–9.
[51] R.A. Saxton, D.M. Sabatini, MTOR signaling in growth, metabolism, and disease, Cell 168 (6) (2017) 960–976, https://doi.org/10.1016/j.cell.2017.02.004.
[52] Y. Zhu, T. Tchkonia, T. Pirtskhalava, A.C. Gower, H. Ding, N. Giorgadze, A. K. Palmer, Y. Ikeno, G.B. Hubbard, M. Lenburg, S.P. O'Hara, N.F. LaRusso, J. D. Miller, C.M. Roos, G.C. Verzosa, N.K. LeBrasseur, J.D. Wren, J.N. Farr, S. Khosla, M.B. Stout, S.J. McGowan, H. Fuhrmann-Stroissnigg, A.U. Gurkar, J. Zhao, D. Colangelo, A. Dorronsoro, Y.Y. Ling, A.S. Barghouthy, D.C. Navarro, T. Sano, P. D. Robbins, L.J. Niedernhofer, J.L. Kirkland, The Achilles' heel of senescent cells: from transcriptome to senolytic drugs, Aging Cell 14 (4) (2015) 644–658, https://doi.org/10.1111/acel.12344.
[53] D. Frasca, Y.B. Saada, D. Garcia, B. Friguet, Effects of cellular senescence on metabolic pathways in non-immune and immune cells, Mech. Ageing Dev. 194 (2021), 111428, https://doi.org/10.1016/j.mad.2020.111428.
[54] C.J. Bruns, G.E. Koehl, M. Guba, M. Yezhelyev, M. Steinbauer, H. Seeliger, A. Schwend, A. Hoehn, K.-W. Jauch, E.K. Geissler, Rapamycin-Induced endothelial cell death and tumor vessel thrombosis potentiate cytotoxic therapy against pancreatic cancer, Clin. Cancer Res. . J. Am. Assoc. Cancer Res. 10 (6) (2004) 2109–2119, https://doi.org/10.1158/1078-0432.ccr-03-0502.
[55] R. Wang, Z. Yu, B. Sunchu, J. Shoaf, I. Dang, S. Zhao, K. Caples, L. Bradley, L. M. Beaver, E. Ho, C.V. Löhr, V.I. Perez, Rapamycin inhibits the secretory phenotype of senescent cells by a Nrf2-independent mechanism, Aging Cell 16 (3) (2017) 564–574, https://doi.org/10.1111/acel.12587.
[56] M.A. Zimmerman, S. Wilkison, Q. Qi, G. Chen, P.A. Li, Mitochondrial dysfunction contributes to rapamycin-induced apoptosis of human glioblastoma cells - a synergistic effect with temozolomide, Int. J. Med. Sci. 17 (17) (2020) 2831–2843, https://doi.org/10.7150/ijms.40159.
[57] W. Günther, E. Pawlak, R. Damasceno, H. Arnold, A.J. Terzis, Temozolomide induces apoptosis and senescence in glioma cells cultured as multicellular spheroids, Br. J. Cancer 88 (3) (2003) 463–469, https://doi.org/10.1038/sj.bjc.6600711.
[58] B. Li, C. Zhou, L. Yi, L. Xu, M. Xu, Effect and molecular mechanism of MTOR inhibitor rapamycin on temozolomide-induced autophagic death of U251 glioma cells, Oncol. Lett. 15 (2) (2018) 2477–2484, https://doi.org/10.3892/ol.2017.7537.
[59] L. Garros-Regulez, P. Aldaz, O. Arrizabalaga, V. Moncho-Amor, E. Carrasco-Garcia, L. Manterola, L. Moreno-Cugnon, C. Barrena, J. Villanua, I. Ruiz, S. Pollard, R. Lovell-Badge, N. Sampron, I. Garcia, A. Matheu, MTOR inhibition decreases SOX2-SOX9 mediated glioma stem cell activity and temozolomide resistance, Expert Opin. Ther. Targets 20 (4) (2016) 393–405, https://doi.org/10.1517/14728222.2016.1151002.
[60] V. Jacevic, E. Nepovimova, K. Kuca, Toxic injury to muscle tissue of rats following acute oximes exposure, Sci. Rep. 9 (2019), https://doi.org/10.1038/s41598-018-37837-4.
[61] V. Jacevic, E. Nepovimova, K. Kuca, Interspecies and intergender differences in acute toxicity of K-oximes drug candidates, Chem. Biol. Interact. 308 (2019) 312–316, https://doi.org/10.1016/j.cbi.2019.05.035.
[62] Z. Chrienova, D. Rysanek, P. Oleksak, D. Stary, M. Bajda, M. Reinis, R. Mikyskova, O. Novotny, R. Andrys, A. Skarka, P. Vasicova, J. Novak, M. Valis, K. Kuca, Z. Hodny, E. Nepovimova, Discovery of small molecule mechanistic target of rapamycin inhibitors as anti-aging and anti-cancer therapeutics, Front. Aging Neurosci. 14 (2022), 1048260, https://doi.org/10.3389/fnagi.2022.1048260.
[63] D. Rysanek, P. Vasicova, J.N. Kolla, D. Sedlak, L. Andera, J. Bartek, Z. Hodny, Synergism of BCL-2 family inhibitors facilitates selective elimination of senescent cells, Aging 14 (16) (2022) 6381–6414, https://doi.org/10.18632/aging.204207.
[64] Z. Novakova, S. Hubackova, M. Kosar, L. Janderova-Rossmeislova, J. Dobrovolna, P. Vasicova, M. Vancurova, Z. Horejsi, P. Hozak, J. Bartek, Z. Hodny, Cytokine expression and signaling in drug-induced cellular senescence, Oncogene 29 (2) (2010) 273–284, https://doi.org/10.1038/onc.2009.318.
[65] M. Kosar, J. Bartkova, S. Hubackova, Z. Hodny, J. Lukas, J. Bartek, Senescence-associated heterochromatin foci are dispensable for cellular senescence, occur in a cell type- and insult-dependent manner and follow expression of P16(Ink4a), Cell Cycle Georget. Tex. 10 (3) (2011) 457–468, https://doi.org/10.4161/cc.10.3.14707.
[66] M. Feoktistova, P. Geserick, M. Leverkus, Crystal violet assay for determining viability of cultured cells, pdb.prot087379, Cold Spring Harb. Protoc. 2016 (4) (2016), https://doi.org/10.1101/pdb.prot087379.
[67] J. Schindelin, I. Arganda-Carreras, E. Frise, V. Kaynig, M. Longair, T. Pietzsch, S. Preibisch, C. Rueden, S. Saalfeld, B. Schmid, J.-Y. Tinevez, D.J. White, V. Hartenstein, K. Eliceiri, P. Tomancak, A. Cardona, Fiji: an open-source platform for biological-image analysis, Nat. Methods 9 (7) (2012) 676–682, https://doi.org/10.1038/nmeth.2019.
[68] C.A. Schneider, W.S. Rasband, K.W. Eliceiri, NIH image to ImageJ: 25 years of image analysis, Nat. Methods 9 (7) (2012) 671–675, https://doi.org/10.1038/nmeth.2089.
[69] J.T. Litchfield, F. Wilcoxon, A simplified method of evaluating dose-effect experiments, J. Pharmacol. Exp. Ther. 96 (2) (1949) 99–113.